INVESTIGATING THE AQUEOUS BEHAVIOR OF D-GLUCOSE, D-FRUCTOSE AND D-ALLULOSE BY MOLECULAR DYNAMICS (MD) SIMULATIONS AND NUCLEAR MAGNETIC RESONANCE (NMR) RELAXOMETRY

A THESIS SUBMITTED TO
THE GRADUATE SCHOOL OF NATURAL AND APPLIED SCIENCES
OF
MIDDLE EAST TECHNICAL UNIVERSITY

BY

ZINNUR YAGMUR BALABANLI

IN PARTIAL FULFILLMENT OF THE REQUIREMENTS
FOR
THE DEGREE OF MASTER OF SCIENCE
IN
FOOD ENGINEERING

JANUARY 2022

Approval of the thesis:

INVESTIGATING THE AQUEOUS BEHAVIOR OF D-GLUCOSE, D-FRUCTOSE AND D-ALLULOSE BY MOLECULAR DYNAMICS (MD) SIMULATIONS AND NUCLEAR MAGNETIC RESONANCE (NMR) RELAXOMETRY

submitted by **ZİNNUR YAĞMUR BALABANLI** in partial fulfillment of the requirements for the degree of **Master of Science** i**n Food Engineering, Middle East Technical University** by,

Prof. Dr. Halil Kalıpçılar
Dean, Graduate School of **Natural and Applied Sciences** _____

Prof. Dr. Serpil Şahin
Head of the Department, **Food Engineering** _____

Assoc. Prof. Dr. Halil Mecit Öztop
Supervisor, **Food Engineering, METU** _____

Assist. Prof. Dr. Beste Bayramoğlu
Co-Supervisor, **Food Engineering, Izmir Institute of Technology** _____

Examining Committee Members:

Prof. Dr. Serpil Şahin
Food Engineering, METU _____

Assoc. Prof. Dr. Halil Mecit Öztop
Food Engineering, METU _____

Assist. Prof. Dr. Beste Bayramoğlu
Food Engineering, Izmir Institute of Technology _____

Assoc. Prof. Dr. Emine Deniz Tekin
Computer Engineering, Türk Hava Kurumu University _____

Assist. Prof. Dr. Antoine Marion
Chemistry, METU _____

Date: 17.01.2022

I hereby declare that all information in this document has been obtained and presented in accordance with academic rules and ethical conduct. I also declare that, as required by these rules and conduct, I have fully cited and referenced all material and results that are not original to this work.

Zinnur Yağmur Balabanlı

Signature :

ABSTRACT

INVESTIGATING THE AQUEOUS BEHAVIOR OF D-GLUCOSE, D-FRUCTOSE AND D-ALLULOSE BY MOLECULAR DYNAMICS (MD) SIMULATIONS AND NUCLEAR MAGNETIC RESONANCE (NMR) RELAXOMETRY

Balabanlı, Zinnur Yağmur
Master of Science, Food Engineering
Supervisor: Assoc. Prof. Halil Mecit Öztop
Co-Supervisor: Assist. Prof. Beste Bayramoğlu

January 2022, 81 pages

D-Glucose, D-Fructose and D-Allulose are isomeric monosaccharides, specifically D-allulose and D-fructose are carbon-3 epimers of each other. Although they are very similar in structural properties, physical properties of their solutions and food formulations are observed to be different. This thesis focuses on uncovering the aqueous behavior of these three monosaccharides, by investigating their 10, 20 and 40% (w/w) solutions at the molecular level by molecular dynamics (MD) simulations and NMR relaxometry. Number and occurrence frequency of hydrogen bonds (HB) between sugar-sugar, sugar-water, water-water, radial distribution functions (RDF) of water oxygens around monosaccharide oxygens, and bound water ratio were calculated by MD simulations. Diffusion coefficients of three selected monosaccharides were calculated and measured by both MD and NMR methods. Results showed that, glucose and fructose molecules were not tendent to form both intra and intermolecular HBs with itself or each other at the studied concentrations, allulose was also not tendent to form intermolecular HBs with sugar molecules, but intramolecular bonding was observed to be frequent especially in pyranose forms. For all sugars, sugar-water HBs were present in 100% of trajectory, and glucose was

found to be the most successful to cluster water molecules around and form HBs, while allulose was the one with least water clustering and HB abilities. It was revealed that, epimerization of fructose into allulose improved the intramolecular HB forming tendency of allulose, especially of pyranose forms. RDF results showed that, ring hydroxyl and hydroxyethyl oxygens were better at clustering the water molecules at 0.28nm, than the ring oxygens of all ring forms. β form of glucose was the best to cluster water molecules among all tautomers of all sugars. Configurational changes between fructose and allulose significantly affect the water interaction ability of allulose pyranoses, mainly, *O1, O3* and *O5* were found to be responsible for the decrease in number of sugar-water interactions. In the case of allulose, frequent occurrence of furanose form in aqueous media and improved intramolecular HB of pyranose form supports the findings. For diffusion coefficients, sugar and water diffusion coefficients were in a decrease with respect to increasing concentration, being in a good agreement with the increase in the ratio of bound water molecules with increasing concentration. Also, NMR measurements were sharing the same decreasing trend with calculated values.

Keywords: Hydration Behavior, MD Simulations, NMR Relaxometry, Monomers

ÖZ

D-GLIKOZ, D-FRUKTOZ AND D-ALLULOZ'UN SULU ÇÖZELTİLERDEKİ DAVRANIŞLARININ MOLEKÜER DİNAMİK (MD) SİMÜLASYONLAR VE NÜKLEER MANYETİK REZONANS (NMR) RELAKSOMETRE İLE İNCELENMESİ

Balabanlı, Zinnur Yağmur
Yüksek Lisans, Gıda Mühendisliği
Tez Yöneticisi: Doç. Dr. Halil Mecit Öztop
Ortak Tez Yöneticisi: Yar. Doç. Beste Bayramoğlu

Ocak 2022, 81 sayfa

D-Glikoz, D-Fruktoz ve D-Alluloz izomerik monosakaritlerdir, özellikle D-alluloz ve D-fruktoz birbirlerinin karbon 3 epimeridir. Üç şeker monomerine ait kimyasal yapılar çok benzer olsa dahi sulu çözeltileri ve gıda formasyonlarındaki davranışlarının farklı olduğu gözlenmektedir. Bu doğrultuda, tez çalışması bahsi geçen 3 monosakaritin kütlece %10, 20 ve 40 konsantrasyondaki sulu çözeltilerinin davranışlarını moleküler düzeyde, MD simülasyonlar ve NMR ile incelemeyi hedefler. Sistemlerdeki şeker-şeker, şeker-su ve su-su arası Hidrojen bağ (HB) sayıları, HB açığa çıkma yüzdeleri, su oksijenlerinin şeker oksijenleri etrafındaki çapsal dağılım fonksiyonları ve bağlı su oranları MD simülasyonlar sonucunda hesaplanmıştır. Sistemlerdeki moleküllere ait difüzyon katsayıları ise hem NMR relaksometre ile ölçülmüş hem de MD simülasyonlar ile hesaplanmıştır. Çıktılar sonucunda glikoz ve fruktozun kendi türleri arasında molekül içi ve moleküller arası bağ yapma eğilimi düşük olduğu gözlenmiştir, allulozda ise moleküller arası bağ yapma eğilimi düşük iken molekül içi bağ yapma eğiliminin özellikle piranoz formlarında yüksek olduğu gözlenmiştir. Tüm şekerler zamanın %100'ünde su ile HB yapsa dahi, glikozun en fazla, allulozun ise en az sayıda su molekülünü etrafında

konumlandırdığı saptanmıştır. Fruktozun alluloza epimerizasyonu sonucunda meydana gelen yapısal değişimlerin allulozun molekül içi bağ yapma yeteneğini, özellikle piranoz formlarımda artırdığı saptanmıştır. RFD incelendiğinde ise, halkaya bağlı hidroksil ve hidroksimetil gruplarının, halka oksijenlerine göre suları, HB yapma olasılığı yüksek olan 0.28nm'de daha sık konumlandırdığı gözlenmiştir. Glikozun β formu diğer tüm tautomerlere kıyasla su moleküllerini en fazla yoğunlukla konumlandırmıştır. Fruktozun epimerizasyonu ile meydana gelen değişim sonucunda allulozun piranoz formu için su etkileşimleri önemli boyutta azalmış, bu değişimden O1, O3 ve O5 oksijenlerimdeki değişimin sorumlu olduğu gözlenmiştir. Alluloz'da gözlenen denge durumundaki furanoz yoğunluğu ve piranoz formunda artan molekül içi bağ eğilimi destekleyici bulgulardır. Difüzyon katsayılarının ise NMR VE MD simülasyonlarda konsantrasyonla birlikte azalma trendi anlamında uyumlu olduğu gözlenmiştir, bu durum konsantrasyonla artan bağlı su oranı ile uyumlu kabul edilmiştir.

Anahtar Kelimeler: Hidrasyon Davranışı, MD Simülasyonlar, NMR Relaksometre, Monomerler

Dedicated to Barbaros, Sema and Irmak Balabanlı for their endless love and support…

ACKNOWLEDGMENTS

I would like to express my deepest regards to my supervisor and mentor Assoc. Prof. Halil Mecit Öztop for showing consistent support and patience. He enlightened my academic pathway by being the best role model. I'd also like to present heartful of appreciations to my beautiful co-supervisor Assist. Prof. Beste Bayramoğlu for teaching me to be proficient in GROMACS, helping me and being the kindest role model. I will always be pleased to carry my advisors' heritage through my academic life.

I'd like to thank to my co-workers and friends Zikrullah Bölükkaya, Gökcem Tonyalı Karslı, Serap and Şahin Namlı, Esmanur İlhan, Eda Yıldız, Seray Kahraman, Elif Gökçen Ateş, Ülkü Ertuğrul, Ozan Taş, Emrah Kırtıl and Selen Güner for always being willing to help whenever I got stuck. I'd like to express my gratitude to my best friend Beril Duyu for always being there to discover, to grow and to share the life with me. I'd like to send my special thanks to my husband, beloved Buğra Buğday for motivating me to see the best opportunities.

My kindest appreciation goes to my sister, Irmak Balabanlı who brings endless love, and joy to my life with her beautiful soul. Lastly, I would like to express my deepest appreciation to my parents, Sema and Barbaros Balabanlı, who rose me with patience, sacrifice and unconditional love to reach where I am. They showed me how to be disciplined, hardworking and keep motivated. I always knew that they listened to me, understood me, and guided me to find my best. I hope I can be as successful and loving as my parents someday.

We would like to thank Scientific and Technological Research Council of Turkey (TUBITAK) with grant number 217O089. Simulation method development, production runs and radial distribution analysis were covered under this grant. METU Research and Coordination Unit is also acknowledged since hydration and diffusion analysis were covered under the grant TEZ-YL-314-2021-10728.

TABLE OF CONTENTS

LIST OF TABLES

TABLES

LIST OF FIGURES

FIGURES

CHAPTER 1

INTRODUCTION

1.1 Carbohydrates

Carbohydrates, defined basically as the hydrates of carbon with the general formula of $C_n(H_2O)_n$ or $C_n(H_2O)_{n-1}$, are the most abundant group of organic compounds found in nature. Carbohydrates are often called as saccharides, and classified according to their size containing one, two, up to 10 and hundreds to thousands of structural elements, stated respectively as monosaccharides, disaccharides, oligosaccharides and polysaccharides in expanding order. Hence, carbohydrates found in nature are formed by smaller repeating units and can be in various sizes and conformations (Neuman, 2013). Carbohydrates are one of the main energy reservoirs of nature. They contribute to the biological structures and appear as physically protective substances. Also carbohydrates are substrates of many significant natural, industrial, or biological reactions (Bordat et al., 2004). In that sense, carbohydrate-related research, deeper scientific understanding and novel technological developments related to carbohydrates play a critical role in the production of novel food, pharmaceutical, chemical, or packaging materials (Izydorczyk, 2005).

1.2 Monosaccharides

While dealing with the structural, chemical, and physical properties of complex polysaccharide structures, understanding their monomers provides remarkable outcomes. Monomers of carbohydrates, recognized as monosaccharides, are the

smallest unit of elements that cannot be depolymerized by further hydrolysis to smaller sugars, and known to have highly distinctive structural, physical and chemical properties (Izydorczyk, 2005; Pomata et al., 2009). Also, most of the natural, biological and industrial systems involve reactions or physical interactions of monomers (Schenk, 1998). In that regard, it is crucial to understand the behavior of monomers under various conditions.

1.3 Physical and Structural Properties of Monosaccharides

Structurally, sugar monomers are defined as 3 to 9 carbons containing chiral polyhydroxy aldehydes or ketones. Differently oriented hydroxyl groups are attached to the carbon backbone, determining the type of monomer (Izydorczyk, 2005). They are mainly divided into two groups, in open chain forms as aldehyde containing aldoses and ketone containing ketoses. Even though 3 to 9 carbon monosaccharides are present in literature, most of the naturally observed monomers contain 6 carbons and are called keto or aldo hexoses (Wrolstad, 2012). Aldoses contain the carboxyl group at first and ketoses have it on the second carbon and carboxyl carbons annotated as the reactive centers of the molecules. As an example, Fischer projection of the D-glucose and D-Fructose is provided in Figure 1.1, which appear as an aldo-hexose and ketose-hexose respectively.

There are some distinct properties of monomers arising from their structural attributes that will be explained in the following subsections.

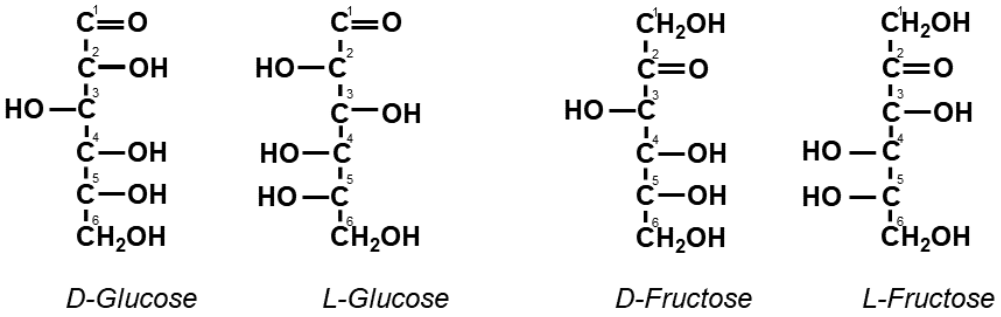

Figure 1.1. Fischer projection of D and L forms of glucose and fructose

1.3.1 Isomerism and Stereoisomerism

Isomerism is the concept of having the same closed formula while having difference in arrangement of atoms, hence displaying a different open formula and configuration. Stereoisomerism, known to be spatial isomerism, is a special case of isomerism in which two molecules have both the same closed formula and the ordering of atoms and the 3D structures of the molecules appear to be different. Interconversion of sugar molecules to their isomers and stereoisomers is possible, by isomerization reactions under the appropriate reaction conditions. Reaction concerns the carbonyl group on C-1 and the adjacent hydroxyl group on C-2. First, aldose form of a sugar changes into an unstable structure triggered by the loss of double bond of carbonyl carbon, resulting a double bond between the first and second carbons. The resulting structure may further evolve into a C2 ketone or a reversed aldehyde. Newly formed aldose and ketoses corresponds to mannose and fructose if the starting monosaccharide is glucose (Fennema, 1996).

Presence of isomers is based on the existence of chiral carbon atoms. Number of possible isomers and stereoisomers of a monosaccharide is determined by the number of chiral carbon atoms. Chiral carbons have four different groups attached to them hence can have two different spatial arrangements resulting in a difference in the 3D structure of the chain (Fennema, 1996). Six carbon containing aldo-hexoses

have 4, and keto-hexoses have 3 chiral centers. In that regard, most of the discovered monosaccharides known to be isomers. For instance, among glucose, fructose, galactose, three of them are isomers having the same closed formula of $C_6H_{12}O_6$ and having different spatial conformations, and glucose and galactose known to be stereoisomers having the same ordering of atoms but different 3D structures.

1.3.2 Epimers and Enantiomers

Stereoisomerism led the formation of epimers and enantiomers as special cases for monosaccharides.

Enantiomers formed by reversing the direction of all hydroxyl groups connected to chiral carbon atoms, which yields into formation of the mirror reflection of the molecule. Two different enantiomers of a monosaccharide named as (D) and (L). A sugar belongs to (D) family if the OH group attached to the highest numbered chiral carbon is written to the right in a *Fischer Projection* notation, and vice-versa (El Khadem, 1988; Izydorczyk, 2005). D forms are abundant over L forms of sugars in nature (Fennema, 1996). D and L forms of glucose and fructose are displayed in Figure 1.1.

Epimers (or diastereoisomers) are formed by reversing only one of the hydroxyl groups connected to a chiral carbon, resulting in the formation of two different monosaccharides. For instance, D-glucose and D-galactose are C-4 epimers.

1.3.3 Anomerism, Mutarotation and, Tautomerism

In aqueous environment monosaccharides are not found in open chain form (<1% for most monosaccharides), since it is not energetically favorable, and they prefer to interchange between the various cyclic forms containing 5 or 6 ring elements called pyranose or furanose rings due to the configurational stability (Izydorczyk, 2005).

Both pyranose and the furanose rings occur by the intramolecular nucleophilic attack to the carbonyl carbon by the backbone hydroxyls. Furanose and pyranose ring formation mechanism of aldoses and ketoses are different from each other and unique. The aforementioned mechanisms and all of the resulting structures are depicted in Figure 1.2 for glucose and Figure 1.3 for fructose being representative for an aldose and a ketose. Mechanism of the reaction affects the final product and leads formation of anomeric or tautomeric monosaccharides, i.e., two concepts appearing only in the cyclic forms of monosaccharides (Eliasson, 2017).

Anomer monosaccharides are recognized as stereoisomers in ring form and differ only in the rotation of the hydroxyl group of the carbonyl carbon with respect to the ring plane. For the D forms of monosaccharides, if the hydroxyl group of anomeric carbon is located above the ring it is called as the β anomer, if it is located below the ring the anomer is the α, as can be observed on Figure 1.2 and 1.3 (Izydorczyk, 2005). Vice versa is valid for L forms.

In solutions α and β anomers of pyranose and furanose rings are found together with the open chain form at a dynamic equilibrium. The process of interchanging between the structures is called the mutarotation(Eliasson, 2017). The reaction takes place ta an energetic cost by whether intramolecular transfer of protons or utilization of water molecules in the proton transfer (Silva et al., 2006).

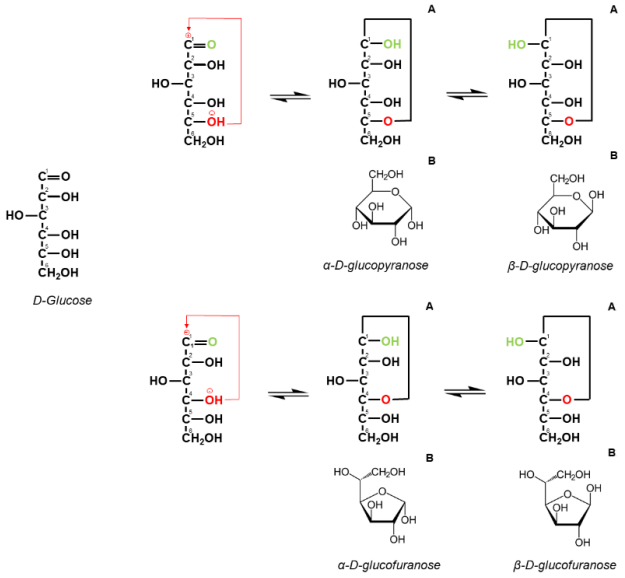

Figure 1.2. Formation mechanism of pyranose ring from D-Glucose. Resulting structures were presented in Fischer (A) and Haworth (B) Projections

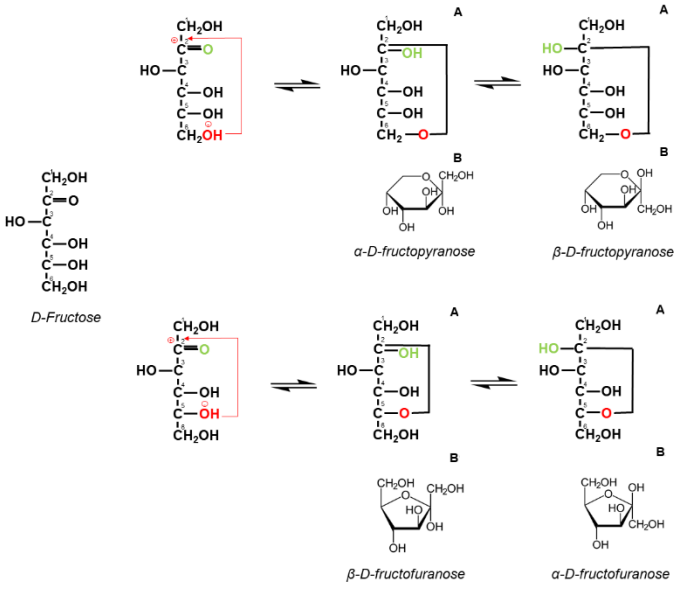

Figure 1.3. Formation mechanism of pyranose ring from D-Fructose. Resulting structures were presented in Fischer (A) and Haworth (B) Projections

Ability of monosaccharides to display all α and β forms of pyranose and furanose rings in the solution at equilibrium is called the ***tautomerization***. Percent distribution of various tautomers depends on the kinetic and thermodynamic state of the system. For example, usually two furanose forms of which sugar are known to be kinetically favored, and two pyranose forms are thermodynamically favored, hence resulting an equilibrium distribution (El Khadem, 1988). Appearance frequencies of tautomers also depend on the type of the solvent. For instance, glucose pyranoses are known to fit better into the tetrahedrally arranged water hydrogen bond lattice hence it is favorable over the other forms (Izydorczyk, 2005).

1.3.4 Aqueous Conformation

Haworth and Fischer projections provide detailed structural information; however, they are not robust enough to display the conformation of the molecule in aqueous solutions. It is discovered that both the furanose and pyranose rings are not flat in their solvated forms and carbon-to-carbon and carbon-to-oxygen atoms in the ring tend to rotate , resulting in various 3D conformations of the ring (El Khadem, 1988; Fennema, 1996; Izydorczyk, 2005).

Pyranose rings display 5 different forms named as *Chair, Boat, Half-Chair, Skew and Sofa forms* (El Khadem, 1988). In chair form a horizontal reference plane is defined by the ring oxygen, C-2, C-3 and C-5. C-1 and C-4 are located outside the plane in different directions resulting in a chair like structure. If C-4 is at the top, the structure is named as $^{4}C_{1}$, and $^{1}C_{4}$ if vice versa. In boat structure a refence plane is formed by four atoms in the ring and the remaining two points outwards the plane being in the same direction. In the case of half chair, reference plane is defined by four contiguous atoms and remaining two are folded up and down the plane, resulting in 12 different structures (Izydorczyk, 2005). All forms are displayed in Figure 1.4.

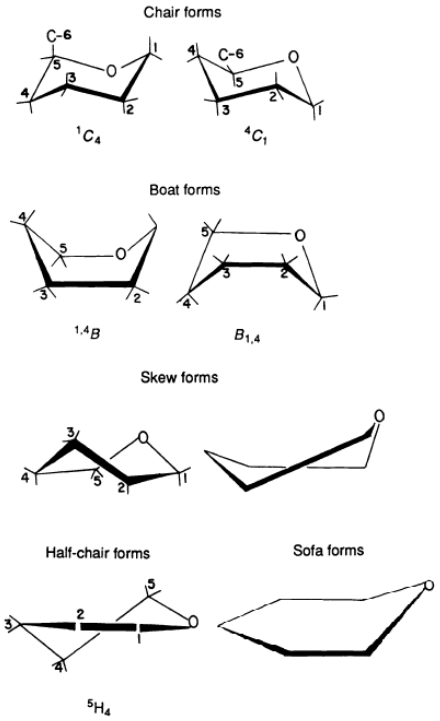

Figure 1.4. Configurational forms of pyranose rings in water (Izydorczyk, 2005)

Even though there are many discovered configurations, the configuration(s) with the minimum free energy is favorable. Free energy is accounted with the bond angles and lengths, van der Waals and electrostatic interactions, steric effects, hydrophobic interactions and the effects of H-Bonding and solvation (Izydorczyk, 2005). Hence it is a huge area of study for each of the monomers. For instance, in the case of glucose, it is found that, $^4C_1$ conformer of the β anomer is favored since it has the ability to bring all the bulky groups connected to ring into minimum contact (El Khadem, 1988; Eliasson, 2017).

Furanose rings display basically two configurations as envelope and the twist, a single configuration of each type is provided in Figure 1.5 as an example. However both of the exemplified forms contain 10 other possible conformers, which makes furanose configuration a complicated phenomenon (Izydorczyk, 2005).

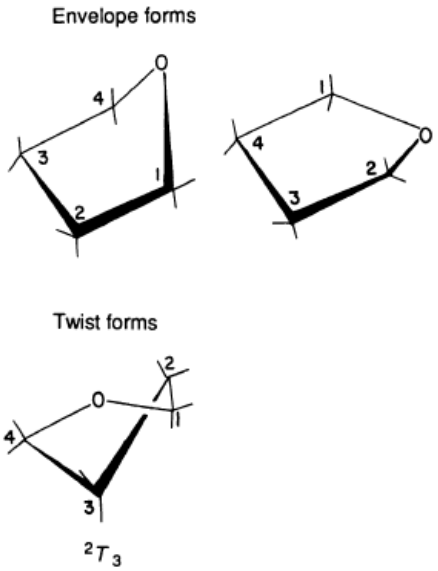

Figure 1.5. Configurational forms of furanose rings in water (Izydorczyk, 2005)

1.3.5 Aqueous Behavior of Monosaccharides

Monosaccharides when solvated and physically interact with water, greatly affect the dynamical properties of pure water. Significant physical interactions that take place during solvation are water-sugar and sugar-sugar H-bonds. It is known that there is a complex interplay among them. Water in pure form adopts a H-Bond lattice with a coordination number around 3. Upon insertion of the monomers, appealing availability of the carbohydrate hydroxyls motivates water molecules to form sugar-water bonds, which are more desirable than water-water bonds. The reason behind the appealing properties of carbohydrates stated as their ability to form acceptor HBs with water. Acceptor HBs can be formed in two equivalent ways since a water molecule has two hydrogens, where there is only one available H atom in donor HBs (Lee et al., 2005). The observed phenomenon disrupts the HB lattice of pure water up to some degree depending on the concentration and possible conformations of the tautomers in aqueous solutions. Together with that with the addition of monomers,

free water molecules attach to the sugar molecules resulting in an increase in the portion of the bound water with slower dynamics (Pomata et al., 2009).

One of the best parameters to describe the molecular mobility and dynamicity of the system is the diffusion coefficient. Diffusion coefficient is extensively utilized to quantitively express the mobility of a species in a system. It is denoted by Eq 1.1. It is in the units of m^2/s.

$$D = \frac{kT}{\pi \beta \eta r} \qquad Eq1.1$$

Where k; Boltzmann constant, T; absolute temperature, β; a numerical constant, η; viscosity, and r; hydrodynamic radius of the diffusing species.

1.3.6 Solution Properties

Once a solute is introduced into solvent, changes taking place in physical properties of the solution system can be classified in two sections. First a change in colligative solution properties, i.e., physical properties that vary with introducing of the solute into the system, is observed. Colligative properties do not depend on the type of the monomer but the quantity is the determining factor. Hence the properties are mathematically interpreted in terms of concentration. Water solutions containing monosaccharides when compared with pure water, have a lower vapor pressure, lower freezing point, and a higher boiling. (Eliasson, 2017).

Secondly, variations in saccharide type, together with its quantity, has an effect on the solution properties. As the type of the saccharide changes, some structural modifications and configurational arrangements take place (Ben Gaïda et al., 2006).

Differences in the aqueous behavior of the monomers can be listed as varying solubilities at same temperature, various hydration numbers and occurrence of different tautomeric ratios and conformers. Moreover, differences in the solution properties can be listed as varying diffusional properties, viscosities and specific volumes (Matlouthi & Reiser, 1995). Sugar bound water molecules known to perform slower dynamics and slower water dynamics are indicated by an increase in the solution viscosity and a decrease in the diffusion coefficients of both water and sugar molecules (Rampp et al., 2000; Sonoda & Skaf, 2007). For instance, among trehalose and sucrose, i.e., two isomeric disaccharides, trehalose was found to have improved water stabilizing properties (N. Ekdawi-Sever et al., 2003). Also, studies involving monosaccharides showed that, viscosities of fructose and glucose solutions were quite different at the same concentration. Also mobility of water around fructose molecule found to be higher than glucose (Mathlouthi & Seuvre, 1988). Together with that, glass transition temperatures of different sugars with varying stereochemistry found to differ (Talon et al., 2004).

It is clear that saccharides, even very similar in structure and conformation, is able to perform different aqueous behavior resulting in varying solution properties.

In this thesis, interaction of water with 3 different monosaccharides; D-glucose, D-fructose and D -Allulose of which the details be given have been studied.

1.3.7 D-Glucose

Glucose, also known as dextrose, grape sugar or starch sugar, is the most frequently occurring monosaccharide in nature, having (D) form in abundance. It is the monomeric unit of cellulose, starch and glycogen. Also, glucose is one of the monomers of sucrose together with fructose, where sucrose is the most significant

industrial sugar (Izydorczyk, 2005). Besides, glucose is not commonly found in nature in free form, except its presence in honey and some fruits.

Structure of glucose was first understood and visualized first by Emil Fischer in 1891, which brought him the Nobel Prize. Glucose was the first monosaccharide to be understood and almost all of the current properties and rules of the monosaccharides were first observed in glucose, then supported by further observations to become rules (El Khadem, 1988).

D-Glucose, with the closed formula of $C_6H_{12}O_6$ and molar weight of 180g, is a 6-carbon containing aldohexose with 4 chiral centers at the C-2, C-3, C-4, C-5. All the hydroxyl groups that are connected to a chiral carbon point right except for the C-3, as depicted in Figure 1.1. Glucose is soluble in water with a solubility of 50.8% (w/w) in pure water at 25ºC. Even though, theoretically glucose has the ability to display 4 tautomers together with the open chain form in a solution, it displays only three tautomers and the most frequently occurring one is the β pyranose anomer (64%), followed by α pyranose (36%) and open chain form (<1%) being not significantly affected by the temperature or concentration (Fennema, 1996; Izydorczyk, 2005).

Glucose can undergo isomerization and be converted to mannose, followed by fructose and other monosaccharides.

1.3.8 D-Fructose

Fructose, also known as levulose, fruit sugar or honey sugar is one of the three most abundant monosaccharides in nature together with glucose and galactose, and it is the principal commercial ketose. In nature D form of the fructose is dominant. It is found in the structure of sucrose in bonded form and in some fruits, vegetables and

honey in free form (Fennema, 1996). It is the sweetest monosaccharide hence it is commercially produced to be used as a caloric sweetener in food formulations.

Its discovery reaches back to 1847, however, chemical interpretation and the explanation of its relation with glucose is found by Fischer on the late 1800s, just like glucose (American Chemical Society, 2017).

D-fructose, being ketose isomer of D-glucose is a 6-carbon containing ketohexose, and it contains 3 chiral carbon atoms located at the C-3, C-4 and C-5. All the hydroxyl groups attached on the chiral carbons point right besides C-3, pointing left. It is soluble in water with a solubility of 80.2% (w/w) at 25ºC. In its solutions it displays three of its tautomers named as β pyranose (75%), β furanose (21%), α furanose (4 %) and open chain form (<%1) (Izydorczyk, 2005).

1.3.9 D-Allulose

Allulose, with its other name Psicose, is a rare sugar, i.e. a monosaccharide being rare in nature as defined according to the International Society of Rare Sugars (International Society of Rare Sugars, 2019). It is discovered that while being 30% less sweet than sucrose, it holds a caloric value of 0.39 kcal/g which corresponds to the 3% of the sucrose's. It also holds some functional properties such as antioxidative effect, neuroprotective properties and ability to reduce blood glucose levels (Ates et al., 2021; Fukada et al., 2010; Li et al., 2018). Accordingly, it is a Food and Drug Administration FDA approved food additive.

Structural properties of D-allulose reveal that it is C-3 epimer of fructose, as depicted in Figure 1.6. Hence it is a 6-carbon containing ketohexose and just like D-fructose it contains 3 chiral carbon atoms located at the C-3, C-4 and C-5. Different from D-fructose, all hydroxyl groups attached on the chiral carbons point right in Fischer Projection. Since allulose is not found in foods in high amounts, it is usually

artificially synthesized. It can be synthesized by epimerization of fructose by enzymes or biotechnological techniques (Li et al., 2018). It is soluble in water, and the concentration of its saturated solution is 72% (w/w) at 25°C. It shows tautomerization and reveals 4 of its tautomers with the open chain form in the solution; α furanose (39%), β furanose (15%), α pyranose (22%), β pyranose (24%) and open chain forms (<1%) (Fukada et al., 2010).

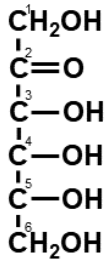

D-Allulose

Figure 1.6. Fischer projection of D-allulose

1.4 Basics of Computer Simulations

Computer simulations involve the concept of utilizing from computer as if it is the virtual laboratory where the variables, the essential rules of its behavior and external conditions are defined by the researcher. Bringing such a mechanism alive requires observation, understanding, consistent assumptions, theoretical expression and the technology. Simulating a system starts from deep observation of the behavior of a system. After having a clear picture of the system behavior, next step is to express the phenomenon by a theory, under correct assumptions. The language of computing science is mathematics; hence system behavior is described by the unique tools of mathematics. By the known attitude of system, its further reactions under certain conditions are predicted, observed measured and evaluated. Procedure of calculation is an art of intelligence, since there is a precise optimization between the cost-

effective interpretation of theory which requires extensive technological knowledge, and minimizing the approximations to create a real-like simulation by interpreting the non-ideal behavior of nature (Rapaport, 1995).

Computer simulations, are widely applicable almost in all areas of science involving the social sciences, economics, material sciences or biological sciences. For instance, materialistic simulations can be composed of nano to macro scale involving even a single atom or billions of it, and can be simulated for femtoseconds to microseconds. Even though construction of a simulation system and a pathway is a challenging process which may require hundreds of years of consistent discovery and hard work, it brings noticeable advantages. By the computer simulations, unreachable or costly real-life systems, can be visualized and understood, behavior of such systems can be predicted under various conditions, risky conditions can be safely tested and mechanism of unforeseen events such as reactions can be unrevealed. Hence, computer simulations are robust tools to understand and uncover the phenomenon that take place at macro to micro and even at atomistic levels (Ma et al., 2017)

1.5 Molecular Dynamics Simulations

Among various areas, sizes and systems that simulations can be applied, Molecular Dynamics simulations is a special area of interest in materialistic simulations. MD simulation systems are many-particle systems sized from nano to micrometer scale and utilizing from numerical integration of the classical theory of Newton's Law of Motion to model the motion of atoms and molecules to generate a dynamical trajectory. Hence it is attributed as a classical method of simulation (Lesar, 2013). MD simulations has a significant role on the understand or predict the structural, dynamic and thermodynamic properties of molecular systems (Braun et al., 2019).

1.6 Implementation

1.6.1 Expression of the system

In the application of MD simulations, molecules are modeled as mass and electric charge carrying point particles that are connected to each other via mechanical spring-like bonds that cannot be broken or reformed. Bonds are free to rotate, and molecules are free to display translational and rotational motion as a result of their interaction with each other (Braun et al., 2019). Molecular structures were introduced into simulation systems via "structure files". Name of the atom, its location and the bonding type and order is defined in the files. Hence computer gets the information that which atoms are connected in which order. Common molecular structures, amino acids, biomolecules, saccharides and some polysaccharide complexes were defined and stored in protein data bank which is an open access platform offering structure files (Berman et al., 2002). For uncommon or unique molecular structures, various programs are present for creating structure files, such as Avogadro and Materials Studio (Hanwell et al., 2012).

1.6.2 Potential Energy Calculation and Force Fields

The potential energy of a molecule is defined as a function of the atomic coordinates in 3D. Potential energy containing the bonded potentials (bond stretching, angle bending, bond rotation, i.e., torsion potentials) and non-bonded potentials (van der Waals and electrostatic potentials) were computed for a given initial structure by using the predefined parameters and electric charges.

Parameters that define the properties of their interactions were known as "forcefield files". Hence batch of aforementioned predefined parameters is called a forcefield, it is developed by the theoretical chemists based on experimental findings and elaborate calculations (Braun et al., 2019). Theoretical expression behind the calculation of potential related to each interaction is presented in Table 1.1.

Development of force field parameters and their validation by experimental or quantum mechanical data is an area of research, and there are various force fields packages with different notations, parameters and energetic expressions to be used in MD simulations. Different force fields were initiated by different research groups, and they are still in the process of development by researchers contributing worldwide, for instance Charmm, GROMOS, General Amber Force Field (GAFF) are some examples.

Choice of forcefield is a critical decision since all the force fields are built on approximations that aim to optimize between the accuracy and transferability. Forcefields generally differ in the evaluation of molecular residues, assignment of partial charges, expression of the energy functions and the parameters used, in that case, transferability, defined as the usability of the same set of parameters for related molecules, is hard to achieve. For instance, some are better at describing proteins, some are better at carbohydrates, lipids or membrane systems. Selection has to be done according to the representability of the force field on the type of the system.

Charmm36 force field has been utilized in the study. It is an all-atom force field in which each of the atoms are represented separately in the force field. More specifically Charmm36m force field is used (Huang et al., 2016).

Table 1.1 Theoretical background of the potential energy elements (Leach, 2001)

Potential Energy Element	Representative Equation	Force Field Described Parameters
Bond Stretching Potential	$\sum_{bonds} \frac{k_i}{2}(l_i - l_{i,0})^2$ l: *distance between two bonded atoms*	$k_i\,, l_{i,0}$
Angle Bending Potential	$\sum_{angles} \frac{k_i}{2}(\theta_i - \theta_{i,0})^2$ θ: *angle between two bonds*	$k_i, \theta_{i,0}$
Torsion Potential	$\sum_{angles} \frac{V_n}{2}(1 + \cos(n\omega - \gamma))$ ω: *dihedral angle*	V_n, n, γ
van der Walls Potential (Lennar-Jones Potential)	$\sum_{i=1}^{N}\sum_{j=i+1}^{N} 4\varepsilon_{ij}\left[\left(\frac{\sigma_{ij}}{r_{ij}}\right)^{12} + \left(\frac{\sigma_{ij}}{r_{ij}}\right)^{6}\right]$ r_{ij}: *distance between atom pairs* N: *total number of atoms*	$\varepsilon_{ij}, \sigma_{ij}$
Electrostatic Potential (Coulomb Potential)	$\sum_{i=1}^{N}\sum_{j=i+1}^{N} \frac{q_i q_j}{4\pi\varepsilon_0 r_{ij}}$ r_{ij}: *distance between atom pairs* N: *total number of atoms*	q_i, q_j

1.6.3 Integration of Newton's Law of Motion

Once the potential energy is calculated, by taking the negative derivative of the potential energy, the force acting on the atoms are computed. Calculation of the force acting on each atom leads the use of Newton's Second Law of Motion to describe the motion of the atoms. Newton's Law is numerically integrated for the given period of time, ranged between femtoseconds to microseconds usually with the timestep of 0.5 to 4.0 femtoseconds. By using the initial locations and velocities of the atoms in the system, it becomes possible to calculate the state for the next time step, yielding a trajectory of molecules and atoms (Leach, 2001). The time step is determined depending on the period of fastest moving atom not to miss any move of atoms or prevent the integration errors that may cause failure of the simulation run.

Integration mechanism of Newton's Law can be performed by various numerical calculation algorithms explained named as Verlet, Velocity-Verlet or Leap-Frog being the most recognized ones. Leap-Frog Algorithm has been utilized in the study. It utilizes from the positions at time t and velocities at time t-Δt/2 to update the position and velocity of an atom at t+Δt/2 (Abraham et al., 2016). Mathematical representation of the method is provided in Eq 1.2 and 1.3.

$$v\left(t+\frac{\Delta t}{2}\right)=v\left(t-\frac{\Delta t}{2}\right)+\frac{\Delta t}{m}F(t) \quad Eq\ 1.2$$

$$r(t+\Delta t)=r(t)+\Delta t v\left(t+\frac{\Delta t}{2}\right) \quad Eq\ 1.3$$

1.7 Running a Simulation

1.7.1 Package Programs

There are various package programs designed to present a simulation environment with easy-to-use functions, preset parameters, protocols, tools analysis and visualization to users. Some examples are AMBER, CHARMM or GROMACS.

Each of the programs have their own commands, language, methods of computation and analysis. Even though interpretation and evaluation of the structure and topology files appear to be different, overall philosophy is the same. GROMACS Package Program version 5.1 is used in the study (Abraham et al., 2016).

1.7.2 Setting a Simulation Box

System to be simulated has to be expressed in terms of simulation tools. The process of preparing the system to simulation involves setting a proper starting state of the targeted system, avoiding highly undesirable conflicts and configurations. Then the force field parameters have to be assigned to each of the elements in the system (Braun et al., 2019).

1.7.3 Setting the Conditions

1.7.3.1 Ensembles

Simulations have to be performed in statistical ensembles that describe the equilibrium behavior for the correct and easy evaluation of the thermodynamic properties of the system. MD simulations can be performed under NVE-microcanonical ensemble (constant number of molecules, volume and energy), NVT-canonical ensemble (constant number of molecules, volume and temperature) or NPT-isothermal, isobaric ensemble (constant number of molecules, pressure and temperature). Selection of the correct ensemble is critical in the equilibration of the physical properties and calculation of the thermodynamic properties.

1.7.3.2 Periodic Boundary Conditions and Cut-offs

Simulation systems appear as just the small representations of real systems confined in the defined finite limits. The effect of the finite limits can be quite important in

such small systems since most of the atoms inside the box will be affected by the presence of walls. In that regard, introducing periodic boundaries that basically cover the simulation box with the space filling arrays of its identical copes would alleviate the problem (Leach, 2001; Rapaport, 1995). Periodic boundary conditions allow more accurate estimation pf the bulk properties by allowing each particle to interact with periodic image of other particles, resembling a continuous system (Braun et al., 2019).

Multiplying a simulation box and letting its elements interact with its copes is likely to create the problem of unrealistic intermolecular interactions, since a molecule can interact with its own copies. In order to prevent this, cut-offs in the calculation of non-bonded interactions are introduced into the system. Cut-offs in simulation systems with periodic boundary conditions have to be smaller than the half of the box length (Braun et al., 2019).

1.7.3.3 Time Step and Simulation Time

Timestep and the length of the simulation is highly critical in a molecular simulation. Timestep of the simulation has to be well adjusted to not to miss any movement in the system. In MD simulations it is generally set as the half of the period of the fastest moving atoms, i.e., 1fs during the equilibration stages. However, in the production run, since system reaches equilibrium, the timestep is generally increased to 2 fs to reduce the computational cost.

Simulation time is also very important, since it determined whether the system reaches both structural and thermodynamic equilibrium, or it covers an enough portion of the phase space to form a robust representation.

1.7.4 Energy Minimization and Assignment of Velocities

Potential energy of a molecule is a multidimensional function that depends on the coordinates of each atom of the molecule. It is also referred as the *potential energy surface* since it creates a 3D surface graph. In MD simulations, the ideal starting structure of a system is desired to be at the global minimum, however it is not reachable since it is impossible to visualize the entire energy surface of a molecule, hence a system. In order to achieve the desired case, local minima of the potential energy in the discovered portion of the system are detected with the use of minimization algorithms (Leach, 2001). By the energy minimization, improper conflicts are overcome and the blowing up of the simulation box (*which is usually caused by the unreasonable large movement of an atom*) is prevented.

There are many minimization methods both utilizing from non-derivative and first order or second order derivative procedures while detecting and sorting the local minima of the potential energy surface. Among all, one of the derivative procedures, the standard procedure of *Steepest Descent algorithm* has been utilized in the study. (Petrova & Solov'Ev, 1997).

Energy minimization helps to obtain energetically minimized structure, however, to start a simulation, initial velocity has to be determined as well. Determination of initial velocities is performed by assignment of random velocities to the atoms according to the Maxwell-Boltzmann distribution.

1.7.5 Equilibration

Before the actual simulation which data will be collected for the evaluation of the physical, thermodynamic and structural properties, an equilibration has to be performed to make sure that the conditions are appropriate, system is at the target state point and unbiased, with respect to the starting configurations and conditions.

NVT simulations involving a thermostat algorithm are utilized for the temperature equilibration and NPT simulations involving a barostat algorithm are utilized for the pressure equilibration. A strong indicator of the equilibrium is the pressure, temperature box volume and density all fluctuating around constant values with minor drifts. However, convergence of the stated properties is not enough to make sure that systems reached equilibrium. There are other properties of system that may converge slower. Those may depend on the system but in most systems fluctuations in Root Mean Squared Deviation, Mean Squared Deviation, Number of Hydrogen Bonds may be strong indicators (Abraham et al., 2016).

1.7.5.1 Thermostat

To simulate a system under constant temperature with NVT (canonical) ensemble, thermostat algorithms are utilized. There are various temperature coupling algorithms. One of the most popular ones is Berendsen. It is a weak coupling algorithm that utilizes first order kinetics. Deviation of the temperature from the desired value is corrected by suppressing the fluctuations in kinetic energy (Abraham et al., 2016). It provides good results in terms of equilibrating the system in an efficient manner. However, it doesn't probe a correct canonical ensemble. Another popular thermostat is, the Noose-Hoover thermostat, which provides strong-coupling with an improved canonical ensemble by manipulating the equations of motion (Hoover, 1985).

1.7.5.2 Barostat

To simulate a system under constant pressure with NPT (isothermal-isobaric) ensemble, barostat algorithms can be utilized. One of the most commonly used ones is the Berendsen weak-coupling barostat. Berendsen barostat provides a first order relaxation by rescaling the box vectors and atomic coordinates.

Another popular one is the strong-coupling algorithm called Parrinello-Rahman Barostat. Similar to Nose-Hover thermostat , the equations of motion are manipulated to achieve a constantly fluctuating pressure (Abraham et al., 2016).

1.7.6 Production Run and Analysis

After making sure that the system reached equilibrium, production run can be performed in order to collect data for analysis and make conclusions. Timestep, frequency of data storage and simulation time can be different than the equilibration protocols to decrease the computational cost.

Outputs of the simulation is analyzed for the desired properties which may potentially involve physical, thermodynamic, bonding or energetic properties.

1.8 Molecular Dynamics Simulations and Carbohydrate Systems

Carbohydrates have gathered huge interest due to their role in biological and industrial applications. Many researchers put their efforts to develop carbohydrate representing MD/MM force fields and it is still in the process of development (Gaweda & Plazinski, 2019; MacKerell et al., 2010; Plazinski et al., 2016; Plazinski & Plazinska, 2017). MD simulations have the strong potential to provide molecular information at moderate cost (Gaweda & Plazinski, 2017, 2019; Maugeri et al., 2017; Pandey & Mallajosyula, 2016).

Glucose, solely has been a topic of interest to be elucidated by MD simulations, and non-surprisingly it was the first one to be elucidated. Its aqueous conformation, hydration behavior, mutarotation and conformational properties has been studied by many researchers. Molteni & Parrinello (1998), analyzed the hydrogen bonds around the anomeric site of α and β glucose and revealed that although being the least

abundant anomer in water; the α anomer, tended to bind water molecules more tightly and β anomer allowed the water molecules to flow in a disorderly manner around its anomeric site. In another study, glucose was compared with various monomers and dimers in terms of hydration number and water activity by using density measurements (Gharsallaoui et al., 2008).

Similar to glucose, fructose is also a widely studied monosaccharide. Its improved sweetness, different solubility, crystallization rate and tautomerization has triggered the attention of many researchers. In the work by Pomata et al. (2009), MD simulations of aqueous fructose solutions up to 70% (w/w), have been carried out. Water and sugar motions were traced for different systems. Results showed that for concentrations over 45%, sugar molecules formed H-bonded clusters that yielded a heterogenous percolated-like system involving patchy regions of water. Sonoda & Skaf, (2007), studied concentrated fructose solutions and found out that water dynamics were similar to that of protein hydration chamber.

A naturally occurring sugar solution of mostly glucose and fructose, i.e., honey, also gained attention of researchers. MD simulations were utilized to compare the crystallization properties of different honey samples and the results of the structural and energetic analysis showed that the certain ratio of sugar types highly affected the crystallization tendency of honey (Ma et al., 2017; Naik et al., 2019).

In addition to monosaccharides, there are many studies focusing on comparing the aqueous behavior of dimeric saccharides sucrose, trehalose, and maltose since they are homologous dimeric saccharides with the same molecular formula differing in the conformation, and especially due to their bioprotective properties. Lerbret et al. (2005), compared the solutions ranging from 4 to 49% (w/w) for the three sugars and due to the localization of water molecules, the number of hydrogen bonds and geometries of sugar molecules trehalose was confirmed to have superior water interaction and stabilization properties over sucrose and maltose. Similarly, Heid et

al. (2019), analyzed water dynamics and showed that trehalose was more successful in retarding the motion of water to a larger extent than the other homologs. Differently, Ekdawi-Sever et al. (2001), studied the physical properties of aqueous sucrose near glass transition temperatures and results of the H-bond and diffusion coefficient analysis revealed valuable information about the aqueous behavior and water interaction of sucrose.

1.9 Objectives of the study

This study focuses on uncovering the aqueous behavior of three monosaccharides, D-glucose, D-fructose, and D-allulose, by investigating the phenomenon at the molecular level by MD simulations. These sugars have the same closed formula and very similar structural properties however, they are highly different in their aqueous behavior and physical properties of their solutions (densities, viscosities, solubilities, crystallization tendencies, and crystal structures). Briefly, D-glucose is a dextrorotatory aldohexose; D-fructose and D-allulose are dextrorotatory ketohexoses. All three monosaccharides are isomers and more specifically D-allulose and D-fructose are carbon-3 epimers of each other. Researches focusing on the behavior of different saccharides in food systems have shown that D-allulose had weaker water-binding properties when compared with sucrose in soft candies and it had a significant effect on the textural properties (Ates et al., 2021; Pocan et al., 2021). However, the reasons and the mechanism behind the stated phenomenon were not extensively explained, especially at a molecular level. In that sense, this study focuses on elucidating the reasons behind stated phenomena by hypothesizing that distinct properties of their solutions arose from the differences in their hydration behavior. Accordingly, this study aims to compare the aqueous behavior, by the number of hydrogen bonds formed by both sugar and water molecules, radial distribution of water oxygens around monosaccharide oxygens and other water oxygens, and diffusion coefficients of three selected monosaccharide solutions in their 10, 20 and 40% solutions (by weight w sugar/w water).

CHAPTER 2

MATERIALS AND METHODS

2.1 Molecular Dynamics Simulations

2.1.1 Simulation Materials and Tools

Molecular Dynamics (MD) simulations were performed by the software GROMACS (GROningen MAchine for Chemical Simulation) version 5.1.4 (Abraham et al., 2015, 2016). GROMACS was accessed by the service utilization from National Center of High-Performance Computation (UHeM). Molecular structure files of all monomers except for the pyranose and β-furanose forms of D-allulose were obtained from the RCSB Protein Data Bank, (Berman et al., 2002). Structure files of D-allulose anomers were manually created by the program Avogadro (Hanwell et al., 2012). Force field topologies of each monomer were generated by CHARMM-GUI Input Generator, Glycan Reader and Modeler tool. All monomers involved in this study were defined in the small molecule library of CHARMM (CSML) and structure files were matched automatically with the corresponding topologies (Jo et al., 2008; Park et al., 2019). CHARMM36m force field was used to describe the type of the atoms and interactions in-between (Huang et al., 2016). For solvation TIP3P type water molecules were utilized.

2.1.2 Method of Application

2.1.2.1 Simulation Boxes

Three carbohydrate monomers; D-glucose, D-fructose, and D-allulose were simulated in the aqueous environment by using the classical simulation method of

Molecular Dynamics (MD) simulations. Concentrations were determined to be under the saturation condition of each sugar solution at 25 °C. The sugars were studied in concentration range of 10, 20, and 40% (w sugar/w solution) at 25 °C. Simulation boxes were designed to finally contain constant number of 1,800 molecules involving both water and sugar. While building the simulation systems, tautomerization and resulting equilibrium anomeric ratios of each sugar were considered and systems were built accordingly at 25 °C. Details of the molecule numbers in each system and their division to anomeric ratios are provided in Table 2.1 (Fukada et al., 2010; Köpper & Freimund, 2003; Plazinski et al., 2016).

Table 2.1 Details of molecule numbers in the simulation systems

	Concentration (w/w %)								
	Glucose			Fructose			Allulose		
	10	20	40	10	20	40	10	20	40
AP	8	17	43	-	-	-	4	9	25
BP	12	27	70	14	32	81	5	11	27
AF	-	-	-	1	2	6	8	17	44
BF	-	-	-	5	10	26	3	7	17
S	20	44	113	20	44	113	20	44	113
W	1780	1756	1687	1780	1756	1678	1780	1756	1678
Total	1800	1800	1800	1800	1800	1800	1800	1800	1800
AP: α-pyranose, BP: β-pyranose, AF: α-furanose, BF: β-furanose									
S: Sugar W: water									

2.1.2.2 Solvent Box Preparation and Equilibration

Simulation boxes were prepared first by placing 6,000 to 9,000 TIP3P type water molecules, arbitrarily into a cubic box (Mark & Nilsson, 2001).

First stage was the energy minimization; the energy of the simulation box was minimized by the *Steepest Descent* algorithm. It is flowed by a temperature equilibration; temperature of the systems was equilibrated by a 1 ns simulation in

canonical (NVT) ensemble for 1ns, to 25 °C with a weak coupling thermostat (Berendsen thermostat). Followingly, pressure of the water box is equilibrated in isothermal-isobaric (NPT) ensemble for 1ns, to 1 bar with a weak barostat (Berendsen barostat) (Berendsen, 1991; Petrova & Solov'Ev, 1997). At the end of the protocol, a stable solvent box was obtained, being ready for insertion of sugar molecules.

2.1.2.3 Solution Box Preparation and Equilibration

A specified number of sugar molecules were inserted into the equilibrated water boxes by arbitrarily replacing the water molecules, according to Table 2.1. Once again for the solution simulation box, energy minimization was performed by the Steepest Descent algorithm. System is equilibrated by a temperature equilibration in NVT ensemble for 1ns with Berendsen thermostat, to 25 °C. It is followed by pressure equilibration in NPT ensemble for 1ns with Berendsen barostat, to 1 bar. After the equilibration stage, excessive water molecules were further removed out from the box to achieve the constant total number of 1800 total molecules for each of the cases.

Finally, the pressure and temperature of the new systems are equilibrated once again in NPT ensemble for 1ns with, to 1 bar at 25 °C with the Berendsen thermostat and barostat. The time constant was set as 0.8 for weak temperature coupling and, 1 for weak pressure coupling throughout the equilibration procedure.

2.1.2.4 Production Run

The systems were simulated in NPT ensemble with Nose-Hoover thermostat and Parrinello-Rahman barostat for a total of 50 ns for 10% systems, 70ns for 20% systems and 90ns for 40% systems, at 1 bar 25 °C with time constants of 0.8 for temperature and 40 for pressure coupling (Hoover, 1985; Nosé, 1984; Parrinello & Rahman, 1981)

For all simulation involving the production run, the following parameters were set:

- *Electrostatic interactions were calculated by the Particle Mesh Ewald method with a coulomb radius of 12Å (Darden et al., 1993).*
- *Van der Waals interactions were calculated by using Lennard-Jones potential by smoothly shifting the interactions to zero between 9 and 12 Å.*
- *Newton's Law of Motion was integrated numerically by the leap-frog algorithm with a 1fs timestep for the equilibration simulations and 2fs for the production run (Van Gunsteren & Berendsen, 1988).*
- *Position restraints were applied on the heavy atoms until the production run.*
- *The length, and angles of all the restricted bonds involving the covalent bonds of hydrogens were constrained by the SHAKE algorithm and periodic boundary conditions were applied throughout the simulations (Kräutler et al., 2001).*
- *Initial velocities during the molecules were assigned according to the Maxwell-Boltzmann distribution.*
- *Neighbor lists were generated at every 20 steps of simulation and the center of mass of the systems were re-calculated at every 100 steps.*
- *Periodic boundary conditions were applied throughout the simulation.*

2.1.3 Post Simulation Analysis

2.1.3.1 Energetic and Physical Attributes

Running average values and time evolution of physical and energetic properties involving temperature, pressure, kinetic, potential and total energies, and density are evaluated for the last 20ns of each simulation, to check the correctness and convergence of the simulation systems. Each of the quantities are calculated by the preset functions of the GROMACS. Pressure, temperature, and energy values are

desired to fluctuate around constant values and calculated density is compared with the experimentally measured values.

Time evolution of Root Mean Squared Deviation (RMSD), and Mean Square Deviation (MSD) are investigated throughout the trajectory to determine the physical equilibrium of the system. RMSD and MSD calculations are performed by processing the position data of each atom i with respect to time *t; r_i (t).* RMSD calculates the positional root mean square deviation of selected atoms according to *Eq 2.1*.The structure of selected atoms is compared with a reference structure by least-square fitting, in which the reference structure was taken from the first frame of production run (Abraham et al., 2016).

$$RMSD(t_1, t_2) = \left[\frac{1}{\sum_{i=1}^{N} m_i} \sum_{i=1}^{N} m_i \|r_i(t_1) - r_i(t_2)\|^2 \right]^{0.5} \quad Eq\ 2.1$$

$$N: number\ of\ atoms\ specfied$$
$$m_i: mass\ of\ atoms\ specfied$$

The time evolution of the center of mass mean-square displacement (MSD) is a robust expression to describe the translational mobility of the elements of a system (Pomata et al., 2009). MSD of atoms belong to index group named "A", is calculated from a set of initial and current positions with respect to the expression stated between angular brackets on the left-hand side of *Eq 2.2*, denoting a statistical average (Abraham et al., 2016). Self-diffusion coefficients *(D_A)* of sugar and water molecules were calculated, by *ad hoc* fitting of MSD data, according to Einstein's Diffusion expression i.e. *Eq. 2.2* (Von Bülow et al., 2020). An error value is also calculated by the program, with the diffusion coefficients denoting the difference between the slopes of two halves of the fit interval of MSD.

$$\lim_{t\to\infty} \langle \|r_i(t) - r_i(0)\|^2 \rangle_{i\epsilon A} = 6D_A t \quad Eq\ 2.2$$

2.1.3.2 Hydrogen Bond Analysis

The number of average intra and intermolecular hydrogen bonds (HBs) that is formed by a sugar molecule and the occurrence percentage of HBs between the stated pairs are calculated.

HBs in the system are classified according to the pairwise interactions as *intramolecular sugar interactions*, *intermolecular sugar-water interactions*, *intermolecular sugar-sugar interactions*. The criterion for hydrogen bonds were determined so that the distance between the donor group and acceptor group is less than 0.35 nm, and the angle between the donor, hydrogen, and acceptor is less than 150^{o}, and in such case the water and the sugar molecules were assumed to be tightly bound (Lerbret et al., 2005). Number of HBs between the pairs in classified groups are calculated for each sugar molecule. Number of HBs vs time data are obtained for each of the molecules of interest, with the selected target group.

Collected data were analyzed by Python scripts. The source codes were provided in appendix D. The codes enabled to average the number of hydrogen bonds made by the molecule of interest with respect to time and then average once again, among the molecules of interest to obtain an average number of hydrogen bond per molecule. Value involves both the time and molecules of the group. The code also calculated the occurrence frequency of the HB of interest in the trajectory by a percentage value. In that case, number of timeframes involving the bond of interest are counted and its ratio to all frames are expressed as a percentage.

2.1.3.3 Radial Distribution Functions

Radial distribution functions (RDF) of water oxygens around water (Ow-Ow) and sugar (Ow-Os) oxygens were computed by analyzing the positions of atoms according to *Eq. 2.4* which denoted the radial distribution function of particle *B* around *A*, where nominator is the particle density of type B at a distance *r* from A denoted by the shaded area in the Figure 2.1, and denominator is the particle density

of type B averaged over total area around particles A (gray area), range is generally set to be the half of the simulation box length (Abraham et al., 2016).

$$g_{AB}(r) = \frac{\langle \rho_B(r) \rangle}{\langle \rho_B(r) \rangle_{local}} \quad Eq\ 2.4$$

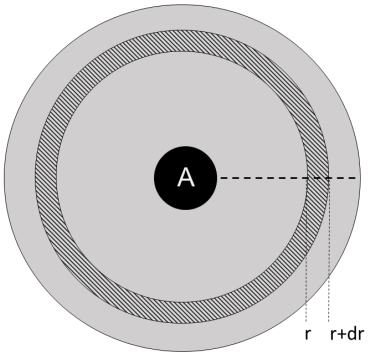

Figure 2.1. Visual representation of radial distribution function calculations

2.2 Time Domain Nuclear Magnetic Resonance Experiments

Self-diffusion Coefficients (SDC) of the sugar solutions were measured. 10%, 20% and 40% (w/w) solutions were prepared by mixing the measured amount of sugar with water. In order to obtain the anomeric equilibrium, solutions were shaked overnight at 25°C. SDC measurements were performed by a stimulated spin echo pulse sequence on a bench top NMR spectrometer operating at a proton frequency of 13.52 MHz (0.32 T) (Resonance Systems GmbH, Kirchheim/Teck, Germany). Spin echo pulse sequence included three 22 us, 90° pulses. The time intervals between the first and the second pulses and between the second and the third pulses were 2 ms and 60 ms, respectively, with an acquisition time of 500 us. The duration of the pulsed gradient field was 1 ms and the gradient strength was 1.66×10^{-2}T/m. Outputs were analyzed by MATLAB.

2.3 Density Measurements

After the preparing the solutions according to the protocol above, density measurements were performed by using a 10mL liquid pycnometer at 25°C.

CHAPTER 3

RESULTS AND DISCUSSION

3.1 Equilibration and Stability

3.1.1 Physical and Energetic Properties and Equilibrium

The running average of temperature during the production run was at 298K with an error of less than 1% for each system. Pressure maintained by Parrinello-Rahman barostat was fluctuating around a constant value.

Total energy and its elements; potential and kinetic energy, were evaluated. During the production run, energies were preserved and were fluctuating around a constant value, which confirmed that the systems were at the energetic equilibrium during the production run. Related figures showing energy fluctuations is provided in appendix A.

3.1.2 Density Validation

Experimentally measured and calculated densities by MD simulations were compared to ensure the representability of the simulation systems and results are reported in Table 3.1. The running average of densities deviated from the experimental results at a maximum error value of 1.7% . Hatcher et al. (2009), showed in their study where they elaborated the representability of the CHARMM force field for various furanoses in solutions containing TIP3P type water molecules and fructofuranose up to 60% concentrations a maximum of 1.4% deviation between the calculated and measured densities and it was considered to be acceptable. In that regard for our system, theoretical density was considered to be consistent with the

experimental results physical and energetic outputs overall validated, simulations form a robust representation.

Table 3.1 MD simulations and experimental density values of solutions

Density (kg/m^3)			
Glucose			
Concentration (w/w %)	Experimental*	Theoretical	Error (%)
10	1027.53 ±*3.12 10^{-4}*	1042.88	**1.5**
20	1071.37 ±*4.80 10^{-}*	1078.8	**0.7**
40	1155.02±*1.62 10^{-4}*	1158.74	**0.3**
Fructose			
Concentration (w/w %)	Experimental*	Theoretical	Error (%)
10	1036.5 ±*5.52 10^{-4}*	1042.78	**0.6**
20	1080.05 ±*2.25 10^{-4}*	1078.9	**0.1**
40	1178.99 ±*3.42 10^{-4}*	1158.95	**1.7**
Allulose			
Concentration (w/w %)	Experimental*	Theoretical	Error (%)
10	1034.01 ±*2.38 10^{-4}*	1040.84	**0.7**
20	1076.38 ±*4.89 10^{-4}*	1074.72	**0.2**
40	1170.14 ±*1.86 10^{-4}*	1149.82	**1.7**
*Standard error is reported with the experimental density to indicate deviation between different samples of replicate sugar solutions.			

3.1.3 Equilibration of the Systems

Time evolution of RMSD and MSD were evaluated to show the convergence of physical mobility of the system. Time evolution of RMSD reached equilibrium in the first 10 ns of the production run and kept fluctuating around a constant value throughout the simulation time with no shift for any of the systems. The results indicated that the initial configuration of the system reached equilibrium (Knapp et al., 2011)..MSD outputs, indicated that the linear increase in MSD was achieved and

the molecular translation reached equilibrium, as presented in Figure 3.1 (Maginn et al., 2019).RMSD figures were provided in appendix B, showing the phenomena discussed above.

Accordingly, due to the absence of unexpected shifts or trends in the time evolution of RMSD and MSD, it was concluded that the systems were physically at equilibrium.

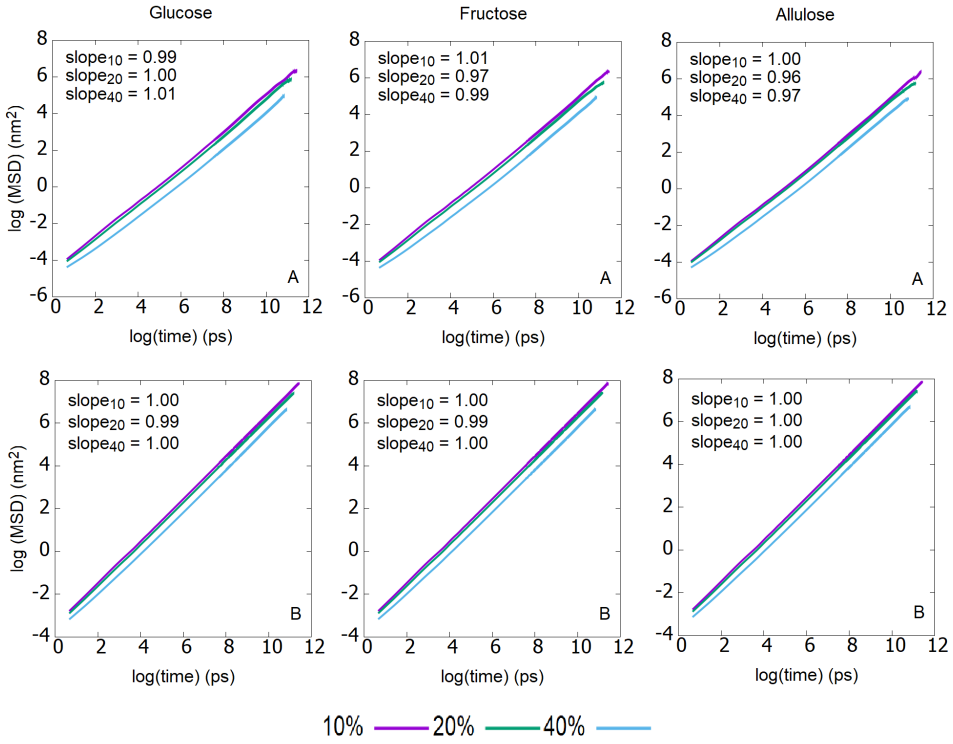

Figure 3.1. Logarithmic plots of mean square displacement of sugar (A) and water (B) molecules in glucose, fructose and allulose solutions

3.2 Diffusion Properties

Determination of transport properties such as diffusivities or viscosities while providing a direct measure of molecular mobility, is a demanding process involving both system-related adjustments and data evaluation (Ekdawi-Sever et al., 2003).

Evaluations were both performed for theoretical calculations and experimental measurements of SDCs.

Critical points while calculating SDCs from MSD can be listed as the selection of the correct simulation ensemble, collecting enough data for a robust evaluation, and deciding on the simulation time and system volume. After successfully achieving a linear MSD graph, linear fitting is to be performed in the meticulously determined region of MSD to best represent the diffusion properties of the system. For the elements of the system to sufficiently cover the available configurational space, it is stated that the square root of MSD should be smaller whether than the box length or radius of gyration of the largest molecule. By that way it will be guaranteed that diffusing molecules traveled a quite good distance and the time in which the properties were evaluated is greater than the correlation of the molecular particles. Also, the slope of the logarithmic plotted MSD-time graph should be equal to 1 to indicate the diffusive region (Maginn et al., 2019). Both conditions were tested in the studied simulation systems and concluded to be satisfied. Logarithmic plotted MSD-time graphs for each system are presented in Figure 3.1. Accordingly, simulation time is considered to be sufficiently long for both sugar and water molecules to reach the diffusive region.

In *ad hoc* fitting of MSD, different intervals were selected for different systems to obtain better fitting properties and to achieve the best representation. 30-80ns, 20-60 ns and 5-45ns for the 10, 20 and 40% (w/w) concentration systems were determined to be suitable for fitting. Theoretical SDCs of both water and sugar molecules are given in Figure 3.2.

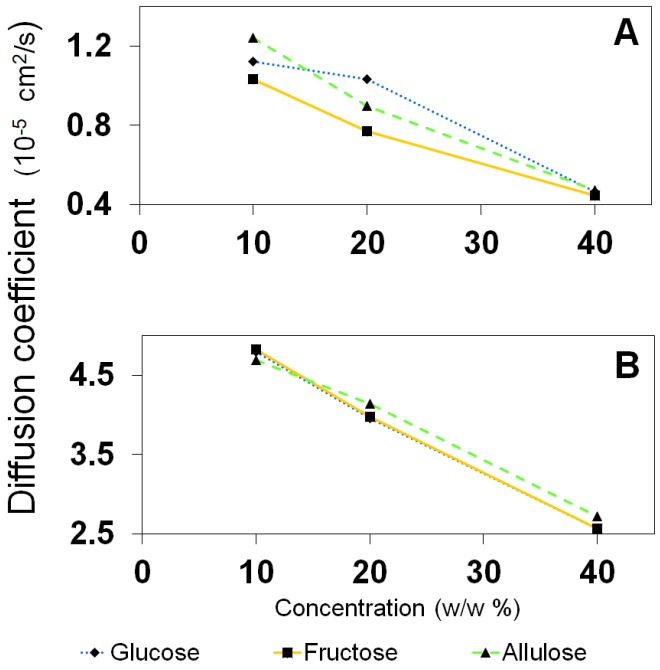

Figure 3.2. Self-diffusion coefficients of sugar **(A)** and water **(B)** molecules in various sugar solutions

For water molecules, theoretical SDCs showed an error maximum of 3.62% overall. The low error margin indicates that the linearity of the MSD plot is achieved and there is almost no difference between the two halves of the fit interval. SDCs of water found in glucose, fructose, and allulose solutions were not meaningfully differing from each other, however, with increasing concentration a linear decrease is observed in SDCs almost being halved as it reaches the highest concentration.

For sugar molecules, there is not a meaningful difference between different monomer solutions having the same concentration. For all systems SDCs were in decrease with increasing concentration. Experimental NMR measurements of SDCs of water also indicated the same conclusions as will be explained.

Calculated water and sugar SDCs, in comparison with the literature values, were in good agreement in terms of the decreasing trend with concentration and had the same order of magnitude for most cases. For instance, fructose solutions at 298K, SDC's

were measured as *2.2* and *0.7 x10*$^{-5}$ m/s^2 at 30 and 50% concentrations (Rampp et al., 2000). In fact, water SDCs deviate up to a considerable extent from the literature values. Values were reaching a maximum of *2.5 x10*$^{-5}$ *cm*^{2}*/s* in systems without or minor solute concentration (Pomata et al., 2009; Rampp et al., 2000; Talon et al., 2004). For the NMR SDCs, the same order of magnitude was obtained for most cases and the difference in values was smaller in comparison with the stated literature values.

NMR and MD SDCs of water molecules were compared with each other by order of magnitude analysis depending on the slope of the logarithmic plot of NMR and MD SDCs. Results are presented in Figure 3.3, the slope of the log-log plots was found to be 0.90 for glucose, 0.73 for fructose, and 0.67 for allulose. As the slope deviates from 1, the difference in the order of magnitude becomes larger for MD and NMR SDCs, therefore analysis indicates that MD and NMR results found to match better for glucose, then it is followed by fructose and allulose. Along with that, diffusion coefficients obtained from distinct methods showed a similar decreasing pattern with increasing concentration in each sugar system.

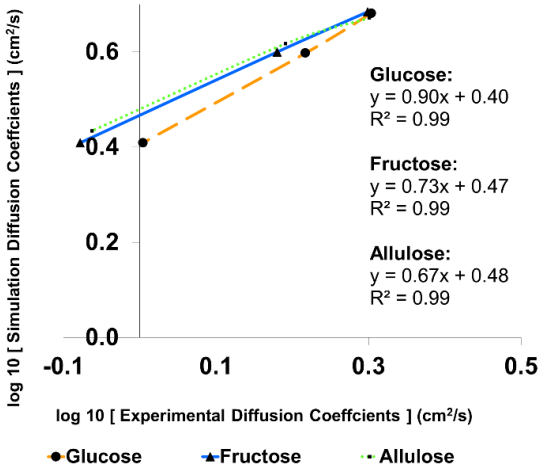

Figure 3.3. Self-diffusion coefficients of water molecules calculated by both methods, log-log

MD and NMR techniques have their critical points, which is likely to yield into errors. For MD simulations it is listed as the nature of force field parameters, water model properties, simulation method-related ensemble properties, system size dependence. Similarly, limitations of NMR measurements are generally the instrument properties. In the case of MD simulations, first of all, force field and water model impacts the diffusion properties since the definition of the molecular structure and the interactions vary (Chen & Smith, 2007). Mark & Nilsson (2001), compared different water models under CHARMM force field, and reported that, TIP3P water molecules, provided diffusion coefficient of $5.8\ x10^{-5}\ cm^2/s$ for pure water systems while the values were $2.9\ x10^{-5}\ cm^2/s$ for SPC/E water model under same conditions. Hence, present results were found to be in a good agreement with the literature values using the same water model and force field.

Secondly, simulation ensemble is stated to be critical in calculating transport properties; it is stated that NVE simulation is favored over NVT and NPT simulations in liquid systems. Since the temperature and pressure are adjusted by a thermostat and a barostat in NVT and NPT ensembles, system dynamics may be significantly affected, which would likely skew the transport properties (Maginn et al., 2019). Another point is that, recovery of periodic boundary conditions after the simulations. Bullerjahn et al., (2020) argue that the conventional tools were not strong enough to provide a suitable trajectory unwrapping to be used in NPT simulations since the approach reverses all jumps through the periodic boundaries up to the most recent time step by using the current box size, in which repeated failures is likely to result in unphysical amplifications of the corrective displacements and dominate them over the actual particle motion.

Selection of the water model, ensemble related fluctuations in the box volume and the unwrapping mechanism are likely to provide skewed results in terms of MSD and certain diffusion properties. Hence, exaggerated diffusion coefficients in comparison with experimental ones are likely to be observed.

It can be inferred that the simulation SDCs were successfully representing the decreasing mobility of molecules with increasing concentration. Skew or exaggeration on the results were most likely to be 'water model' and force field dependent since results match with previous findings that utilized the same tools. (Mark & Nilsson, 2001).

3.3 Hydrogen Bond Analysis

3.3.1 Intermolecular Hydrogen Bonds

3.3.1.1 Sugar - Sugar

Outputs of the average intermolecular sugar-sugar HBs are precisely presented in Table 3.2. Results have shown that for all concentrations and sugar types the average number of HBs that a molecule can form with another sugar molecule ranged between 1 and 1.2, and the percentage of the last 20ns of simulation trajectory involving the HBs ranged between 0.9-1.9%. With increasing concentration, the number of sugar-sugar intermolecular HBs and the % of the trajectory involving the HBs slightly decreased. Even though there is a slight decrease, overall, results present that; a sugar molecule is capable of forming approximately 1 HB with another sugar molecule, and the number of simulation frames that contain at least an HB is around 1-2% last 20ns of simulation for all sugar solutions and concentrations. It was stated that, the infrequent formation of intermolecular sugar bonds arises from the dynamic nature of the system, and favorability of water HBs (Sonoda & Skaf, 2007). In addition, intermolecular sugar bonds was likely to occur as a result of having a common water interaction that brought two sugar molecules in closer contact (Lerbret et al., 2005).

Table 3.2 Average number of intermolecular HBs between the sugar pairs in solution and occurrence percentage in the last 20ns of the of simulation

	Concentration (w/w%)					
	Glucose					
	10		20		40	
Pairs*	Number	Percentage (%)	Number	Percentage (%)	Number	Percentage (%)
AP-AP	1.14	1.91	1.13	1.51	1.03	1.34
BP-BP	1.15	1.73	1.16	1.65	1.06	1.39
AP-BP	1.15	1.84	1.13	1.71	1.04	1.34
	Fructose					
*AF-AF***	-	-	1.09	1.76	1.04	1.66
BF-BF	1.18	1.20	1.20	1.32	1.06	1.17
BP-BP	1.23	1.51	1.20	1.44	1.08	1.19
AF-BF	1.15	1.69	1.12	1.37	1.12	1.04
AF-BP	1.16	1.57	1.12	1.47	1.25	1.02
BF-BP	1.22	1.63	1.18	1.53	1.17	1.06
	Allulose					
AF-AF	1.18	1.20	1.17	1.10	1.08	1.00
BF-BF	1.14	1.36	1.17	1.27	1.08	1.13
AP-AP	1.12	1.23	1.12	1.16	1.01	0.97
BP-BP	1.08	1.22	1.12	1.18	0.96	0.92
AF-BF	1.21	1.47	1.14	1.35	1.09	1.10
AF-AP	1.17	1.45	1.14	1.20	1.06	1.09
AF-BP	1.15	1.39	1.13	1.30	1.05	1.04
BF-AP	1.22	1.54	1.13	1.06	1.08	1.13
BF-BP	1.13	1.44	1.12	1.27	1.03	1.06

**AP: α-pyranose, BP: β-pyranose, AF: α-furanose, BF: β-furanose*
**There is only a molecule in the system so intermolecular interactions couldn't be defined.

3.3.1.2 Sugar - Water

The average number of sugar-water HBs is presented in Figure 3.4. Figure 3.4A firstly highlights that there is a decrease in the number of sugar-water HBs with increasing concentration in all sugar solutions. Secondly, average number of sugar-water HBs is dominated by glucose, followed by fructose and allulose. The trend is preserved for all sugars throughout the concentration range. Moreover, it was found that 100% of the trajectory involved sugar-water HBs for all sugar types among the studied concentration range. Supportively, Lee et al. (2005), obtained the number of HBs per glucose by two methods for 6 weight % binary solutions. 1-Ultrasond technique provided 8.4 at 298K, 2-MD simulations provided 8.8 at 303K. Similarly, Pomata et al. (2009), stated number of HBs per fructose molecule by MD simulations. Values were reaching from 9 to 5.5 by decreasing concentration in the 20 to 50% range (by weight). Calculated values were found to be in accordance with literature. Dominancy of glucose over fructose was also relevant with the literature, which is indicated to be the case in mild concentration limits (Shiraga et al., 2015).

Inspecting the anomers; β-D-glucopyranose had the tendency to form more HBs with water then α-D-glucopyranose, and the trend was conserved with the changing concentrations. The observed phenomenon is previously revealed and explained by the available configurational space around β form of glucose due to equatorial position of the anomeric hydroxyl (Ben Gaïda et al., 2006). Fructose anomers, did not display a difference between their anomers. Allulose anomers, show a trend in which the furanose forms were capable of forming more HBs with water than the pyranose forms.

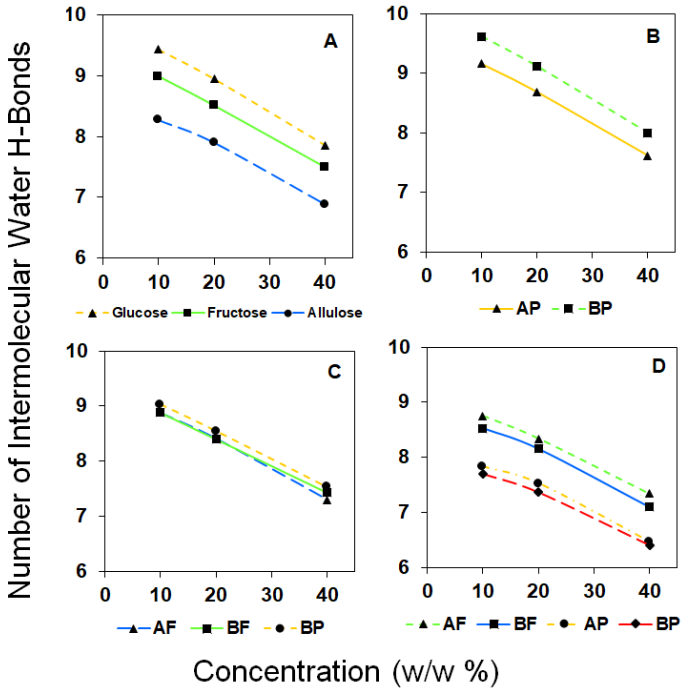

AP: α-pyranose, BP: β-pyranose, AF: α-furanose, BF: β-furanose

Figure 3.4. Average number of sugar-water intermolecular hydrogen bonds with respect to concentration compared in between overall systems (A), glucose anomers (B), fructose anomers (C), and allulose anomers (D)

Moreover, HB behavior of water is analyzed to further explain the decreasing trend observed in the number of sugar-water HBs with increasing concentration. Number of sugar HBs per water molecule and percentage of sugar associated water molecules were calculated accordingly. Results showed that, percentage of the water molecules interacting with a sugar molecule; i.e., percentage of the bound water molecules for all sugars increased with increasing concentration (Table 4). Remarking the presence of sugar-water HBs in the 100% of the analyzed trajectory; it was clearly pictured that water molecules were willing to interact, cover and saturate the solute molecules in the studied concentration range. It is stated that, for the dilute disaccharide solutions sugar molecules are surrounded by wide hydration layers which is compatible with the findings (Lerbret et al., 2005). Stability of the sugar water HBs were found to be higher than the water-water HBs, which explains the motivation of

water molecules to attach to sugars (Lee et al., 2005). Number of HBs formed by a water molecule with sugars in each time frame were also analyzed in the last 20ns. It was observed that, frames containing a single HB with sugar molecules were abundant, contributing to 50 to 85 % of the frames in last 20ns. It was followed by 2 HBs, around 7 to 17 %, 3 HBs, around 0.5 to 3% and 4 HBs being smaller than 1%. It was inferred that most of the water molecules were bound to sugars by a single HB. On the other hand, increasing concentrations resulted in a decrease in the % of the frames containing 1 HB and an increase in the frames containing more than 1 HB for all sugars. It was observed that as the concentration increased, a single water molecule tends to form more than 1 HBs with sugars. Lerbret et al., (2005), stated that with increasing concentration disaccharides tends to share the water molecules rather than having a broad hydration chamber. Considering the decrease in number of HBs per sugar molecule and increase in the ratio of sugar associated water molecules, their claim perfectly explains the observed phenomenon.

Also, ratio of the bound water molecules was the highest in glucose, followed by fructose and allulose (Table 3.3). This result, being consistent with the outputs of sugar HB analysis, suggested that the glucose was the most successful monosaccharide to capture the water molecules, followed by fructose and allulose.

Table 3.3 Percentage of the bound water molecules (%)

Concentration (w/w %)	Glucose	Fructose	Allulose
10	9.72	9.10	8.43
20	19.70	18.34	17.31
40	41.38	38.94	36.40

The results also explain the decreasing trend in SDCs of both sugar and water molecules. It is hypothesized that decrease is well correlated with the frequent occurrence of sugar-water H-bonds. The state of water in a carbohydrate solution can be simply defined as bound to a saccharide or found in the neat fluid in free form (Pomata et al., 2009). In the free state; it is proposed that the water molecules tend

to rearrange themselves by distant angular jumps due to the exchange of HB acceptors, (Laage & Hynes, 2008). However with the presence of dissolved substances such as hydrophilic carbohydrate monomers, sugar-bound water molecules are expected to have slower dynamic properties (Mredha et al., 2013). In that regard, as the number of sugar molecules in the system increases, the fraction of bound water molecules increases, as shown above. This would expect to result in slower water dynamics, and thus lower diffusion coefficients. Supportively, decreasing number of water HBs per sugar molecule, with increasing bound water ratio (indicating mutual sugar bonding to water molecules) tend to result restricted molecular mobility. As a supporting claim, hydrogen bond lifetime was stated to increase with the increasing concentration (Paolantoni et al., 2008).

3.3.2 Intramolecular Hydrogen Bonds

3.3.2.1 Sugar - Sugar

The number of intramolecular HBs per sugar for all glucose anomers was equal to 1 and remained same with increasing concentration. Besides, the percentage of the trajectory involving intramolecular HBs slightly increased with increasing concentration, from 1% to 1.5%. Fructose anomers behaved differently from each other; while the average number of intramolecular HBs of furanoses was slightly above 1, it was slightly below 1 for pyranose. The percentage of occurrence of the intramolecular HBs for furanose forms was around 10 to 12 %, while it was below 1% for pyranose forms. Finally, for the allulose, number of intramolecular HBs were slightly above 1 for β-pyranose, while it was 1 for the other tautomers. In addition, pyranose forms of allulose formed intramolecular HBs more frequently at a percentage of 41-66 % when compared with the furanose forms, which was around 5 to 8%. It is suggested that, intramolecular interactions have an impact on the water or sugar intermolecular interactions. The potential HB sites remain occupied, and intermolecular interactions are restricted accordingly. Even the number of

intramolecular bonds valued around 1 for all sugars, their frequent occurrence can hinder the molecules ability to form intermolecular bonds with water (Lee et al., 2005). Moreover, it affects the aqueous configuration of the molecule and further affects the water localization and ordering properties of water around the molecule (Sonoda & Skaf, 2007).

Table 3.4 Percentage of occurrence of intramolecular hydrogen bonds in the last 20 ns of the trajectory

	Concentration (w/w%)		
	10	20	40
General			
Glucose	0.97	1.55	1.47
Fructose	3.68	3.47	3.66
Allulose	30.3	29.42	29.88
Tautomers*			
Glucose			
AP	0.95	1.52	1.39
BP	0.98	1.56	1.52
Fructose			
AF	10.93	12.41	12.78
BF	12.39	12.58	12.76
BP	0.06	0.06	0.06
Allulose			
AF	7.66	6.87	6.72
BF	8.21	4.47	5.95
AP	49.61	40.54	47.12
BP	64.35	62.85	66.71

*AP: α-pyranose, BP: β-pyranose, AF: α-furanose, BF: β-furanose

3.4 Radial Distribution Functions

RDF between the sugar-water (Ow-Os) and water-water oxygen (Ow-Ow) pairs in the studied systems were elaborately investigated in addition to the HB analysis. Oxygens were either compared one by one or classified according to their site as ring hydroxyl oxygens, ring oxygens, and hydroxymethyl oxygens to compare different

sugar molecules with different configurations. The molecular structures are provided in Figure 3.5.

First general trends were highlighted, secondly elements of each oxygen group were compared within the sugar molecule to distinguish the tautomers. Then glucose oxygens were compared with the furanose and pyranose of fructose to further elaborate the findings of HB analysis. Finally, fructose and allulose's matching forms were compared to highlight the changes due to structural variations.

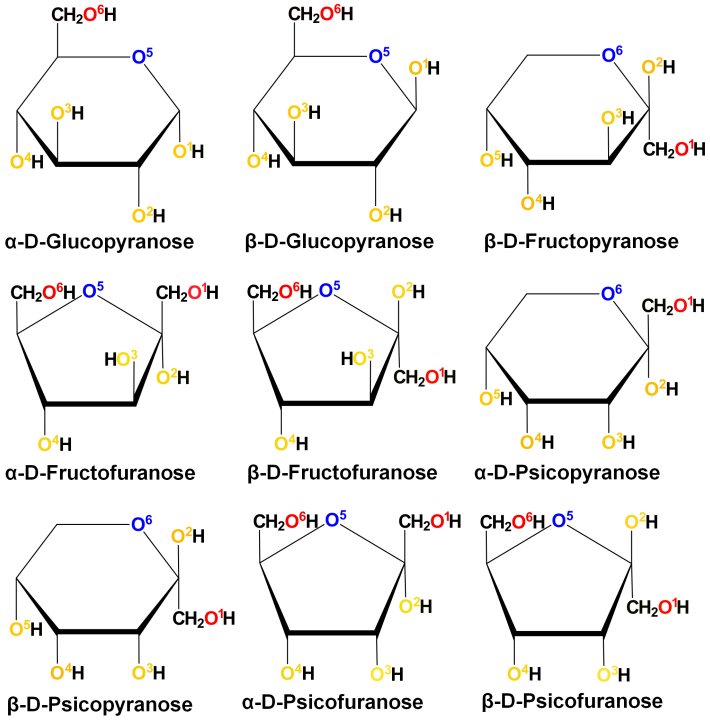

Figure 3.5. Molecular structures of the monomers. The ring hydroxyl oxygens, hydroxymethyl oxygens and ring oxygens are represented in *yellow*, *red* and *blue,* respectively.

3.4.1.1 General Trends

According to the RDF of Ow-Os pairs, any observed behavior was not varying with concentration. Hence all RDF graphs in the following section belong to 40% concentration for a clear representation.

Figure 3.6 shows, RDF of Ow-Os pairs, averaged over all oxygens of an anomer type (α-pyranose, BP: β-pyranose AF: α-furanose, BF: β-furanose) at 40% concentration. Two peaks were observed to appear. 1- a sharp narrow peak at 0.28nm indicating the first hydration shell, 2- a lower, wider peak at 0.55nm indicating the second hydration shell. For the primary peak, separate inspection of each oxygen reveals ring hydroxyl and hydroxymethyl oxygens were responsible for the formations of first hydration shell. The peak corresponded to the first hydration shell consisted of the water oxygens that were readily found to form HBs with the sugar molecules (Pamies et al., 2017). The same peak location observed within the Ow-Ow RDF; shown in Figure 3.7. On the other hand, ring oxygens were observed to cluster water oxygens abundantly around the second hydration shell. This showed that it was not favorable for ring oxygen to form HBs with water when compared with the hydroxyl and hydroxymethyl oxygens.

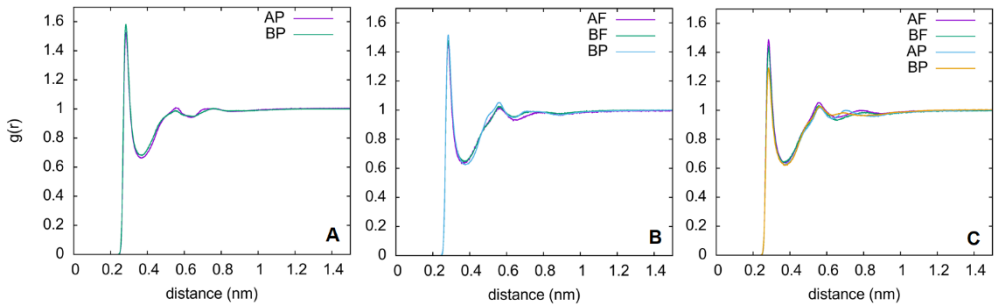

Figure 3.6. Radial distribution functions of water oxygens around sugar oxygens at 40% concentration, averaged over all oxygens, (A) glucose (B) fructose (C) allulose. AP: α-pyranose, BP: β-pyranose AF: α-furanose, BF: β-furanose

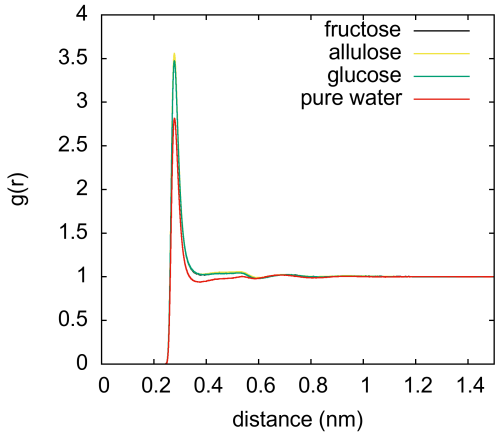

Figure 3.7. RDF of water oxygens around water oxygens at 40% concentration for all sugar types and pure water rdf

3.4.1.2 Sugar Oxygens

Investigation of glucose oxygens showed that Ow-Os RDF mainly differed between the *O1* and *O5* of the two anomers of glucose, as represented in Figure 3.8. For *O1*, α anomer displayed a narrower, smaller peak with a deeper valley and β anomer showed a broader, higher peak with a shallow valley. Together with the RDFs, cumulative analysis of number of hydrogen bonds revealed that, *O1* of β anomer showed higher number of water oxygens in the first hydration shell when compared with the α anomer. Former output is also validated by HB analysis. Results showed that the anomeric hydroxyl oxygen of α anomer more steadily localized the water molecules due to the narrower and deeper peak. However the number of water molecules clustered around β anomeric oxygen was higher. Molteni & Parrinello (1998), also stated that water molecules around anomeric oxygen of β had less residence times than α indicating higher degree of disorder. Outputs of the RDF analysis reinforced the preexisting claims on the increased number of sugar-water HBs in β anomer. Related literature claims that the improved water interactions of β anomer was due to the positional shift from axial in α-form, to the equatorial in β-form. It is known that the oxygen distances between the hydroxyl groups of neighbor

carbon atoms should be compatible with the O-O distance in water HB lattice, for a better fitting into a group of molecules. Equatorial hydroxyl groups were known to interact better with water molecules by providing better physical fitting to the 3D H-bonding structure of water (Galema & Høiland, 1991; Neuman, 2013). Also, the resulting dominancy of β anomer in an equilibrated aqueous solution was considered to be a robust consequence of the improved hydration properties of β anomer, according to the details stated above.

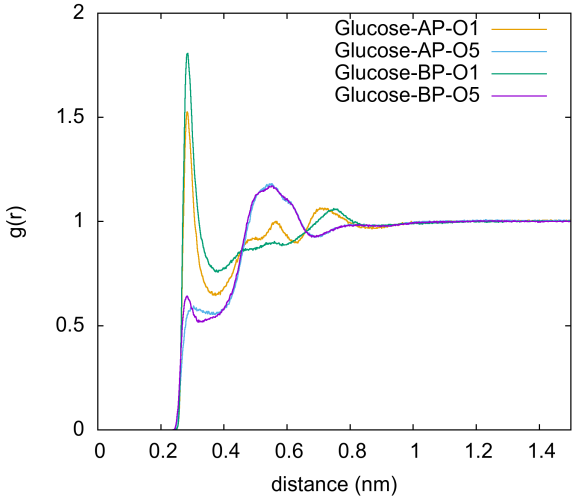

Figure 3.8 Radial distribution functions of water oxygens around the anomeric hydroxyl oxygen *(O1)* and the ring oxygen *(O5)* of glucose at 40% (w/w) concentration. AP: α-pyranose, BP: β-pyranose

Some differences between the behavior of different fructose tautomer's oxygens are described as follows. Ring hydroxyl oxygens namely *O2, O3, O4* in furanose forms and *O2, O3, O4*, and *O5* in pyranose forms, showed distinct behavior.

(1)-For all forms, hydroxyl group oxygen bound to the anomeric carbon, i.e., *O2*, was the least successful to cluster the water oxygens around at 0.28nm and had a more dominant second hydration chamber around 0.55nm. Presence of a closely positioned hydroxymethyl oxygen may affect the water dynamics in that region. For instance, residence time of water molecules near different oxygens of sucrose was

found to be different for different oxygens, indicating distinct water dynamics (Engelsen et al., 2001). See appendix D.

(2)- Among ring hydroxyl oxygens, *O4* in furanose form and, *O4* and *O5* in pyranose form displayed the most stable first hydration shell. This can be explained by the available space in between the hydroxyl groups. The equatorial orientation of *O4* in pyranose form is also likely to fit better into the HB lattice of water (Galema & Høiland, 1991; Lee et al., 2005). See appendix D.

(3)-Ring oxygens, *O5* in furanose and *O6* in pyranose differed in the wideness and height of the peaks. Pyranose ring oxygens displayed a minor first hydration peak and a wider and lower secondary peak while furanose forms only display a secondary peak, being narrower and higher than the pyranose secondary peaks (Figure 3.9B). This indicated that pyranose ring oxygen was clustering a small portion of water molecules at the first hydration chamber. This can be explained by the presence of bulky hydroxymethyl groups around ring oxygen in the case of furanoses. In addition available space is smaller in furanose forms due to smaller ring size (5-membered) (Franks, 1987).

For all tautomers of fructose, hydroxymethyl oxygens dominated the oxygens of other types in hydration properties. The reason suggested is the decreased steric restrictions resulting improved water localization (Livingstone et al., 1977).

In the case of allulose tautomers, among furanose ring hydroxyl oxygens (*O2, O3* and *O4*) *O2* was the least successful hydroxyl oxygens to cluster water molecules at the HB distance similar with the case discussed in fructose. Among the ring oxygens, pyranose ring oxygens displayed a sharp minor peak at 0.28nm while furanose oxygens display a higher second peak around 0.55nm, as shown in Figure 3.9C. While pyranose ring oxygens position a small portion of the water molecules at the HB distance and greater portion in the second hydration chamber, furanose forms only position water molecules in the second hydration chamber. Similar to fructose, available configurational space is also likely to be the reason (Franks, 1987). Finally, hydroxymethyl oxygens of furanose forms showed significantly higher peaks at the

HB distance than the pyranose oxygens, meaning improved localization properties. The output confirms the findings of HB analysis, showing improved H-Bonding in furanose forms. Claims are compatible with the previous findings of molecules containing intramolecular bonds that do not tend to occur frequently in the solution, since water favors to saturate all possible hydration sites (Gaweda & Plazinski, 2019). Gaweda and Plazinski (2019), further stated that intramolecular HBs formed inside the molecules occupy the possible hydration sites and obstructed the water interactions. Also, being unusual among monosaccharides, dominant occurrence of furanose forms that is displayed by aqueous allulose can be related with improved configurational compatibility with water. Figure 3.10A shows Ow-Os RDF for hydroxymethyl oxygens. Figure 3.10B shows the selected top peaks of ring hydroxyls, i.e., *O4* among all tautomers. Peaks belong to furanose observed to be slightly higher.

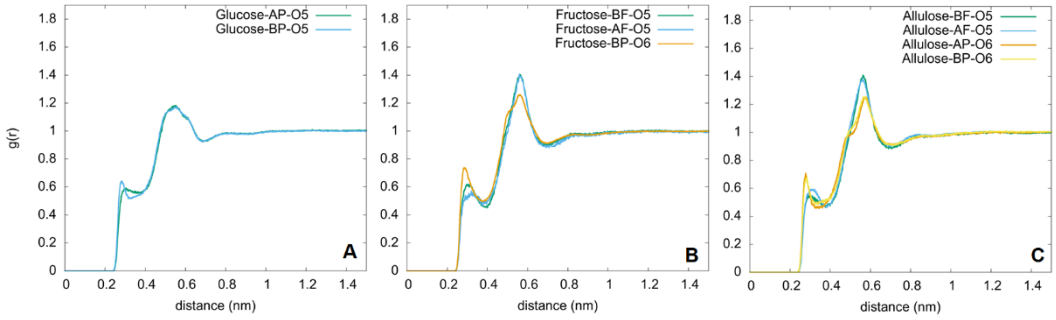

Figure 3.9. Radial Distribution Functions of water oxygens around all ring oxygens of glucose **(A)**, fructose **(B)** and allulose **(C)** at 40% (w/w) concentration. AP: α-pyranose, BP: β-pyranose, AF: α-furanose, BF: β-furanose

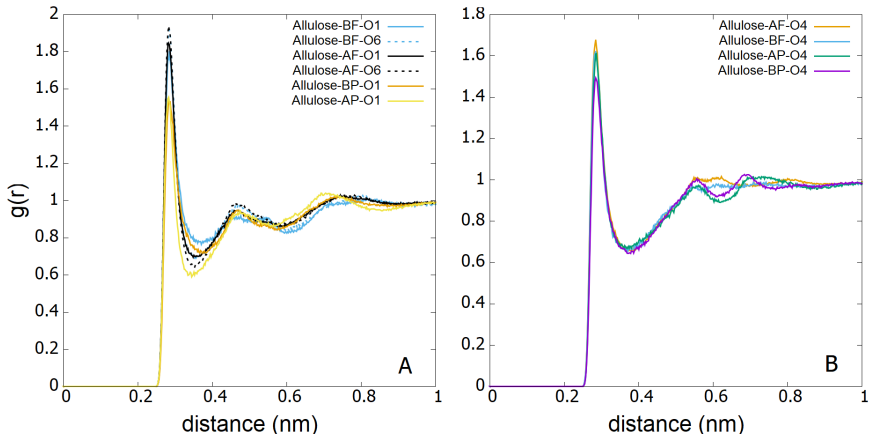

Figure 3.10. Radial Distribution Functions of all hydroxymethyl oxygens **(A)** and *O4* **(B)** of allulose at 40% (w/w) concentration. AP: α-pyranose, BP: β-pyranose, AF: α-furanose, BF: β-furanose

3.4.1.3 Comparison Between All Sugar Molecules

Pyranose forms of all sugars is compared and presented in Figure 3.11. Among the sugar ring hydroxyl oxygens, pyranose forms of all sugars, glucose ring hydroxyl oxygens were better to cluster the water molecules around at HB distance, as shown in Figure 3.11A. Conformational free energy of glucose pyranoses were found to be lower than that of fructose and allulose, this is stated to be a consequence of the improved geometrical compatibility of the molecule to interact with water (Franks, 1987; Gaweda & Plazinski, 2017). Accordingly, it was hypothesized that the presence of hydroxyl groups in each of the ring elements was likely to increase the adaptability of a molecule into the aqueous structure. Finally, a comparison of the hydroxymethyl oxygens (in Figure 3.11B) revealed that the peaks with highest intensity were obtained in the case of glucose, and the lowest was obtained in the case of allulose with a noticeable difference showing that allulose pyranoses were better at locating the water molecules around due to narrower peaks. However, the number of water molecules were lower due to lower peak amplitude. Finding was in

accordance with the HB outputs. Further research comparing the residence times would enlighten the stability water around sugar molecules.

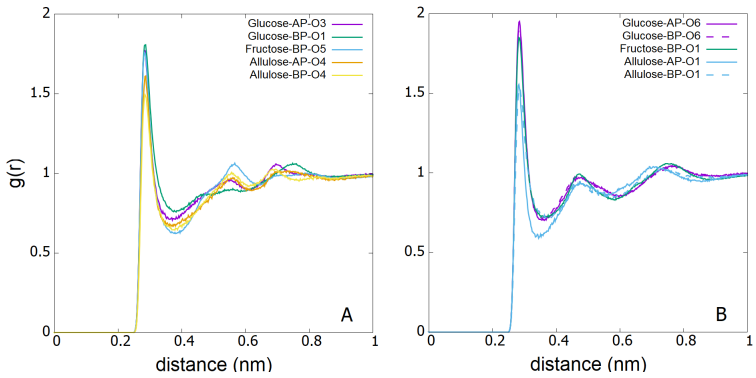

Figure 3.11 Radial distribution functions of water oxygens around ring hydroxyl oxygens (A) and hydroxymethyl oxygens (B) at 40% (w/w) concentration for fructose, allulose and glucose. AP: α-pyranose, BP: β-pyranose, AF: α-furanose, BF: β-furanose

Separately, glucopyranose anomers and, furanose forms of allulose and fructose were compared. Results indicated that for hydroxymethyl oxygens, β glucose *O6* was the top and the *O1* of furanose forms of allulose was the bottom peak. In the case of ring hydroxyl oxygens glucose was observed to be the dominant in the peak height, being higher than almost all oxygens of allulose and fructose. In addition, ring oxygens showed significantly higher secondary peak for allulose and fructose furanoses than glucose pyranose indicating poorer H-Bonding capability with water.

Bringing the comparison of pyranose forms of sugars into a conclusion; glucose was found to be better at clustering more water molecules in the first hydration shell where HB takes place. This was consistent with the HB results as well. Also, secondary peaks when compared between the ring, hydroxyl and hydroxymethyl oxygens of all sugar types, fructose and allulose peaks were sharper and higher than glucose in general. In that case, it can be concluded that the HB lattice of pure water, in absence of any solvents was preserved better in the case of glucose, and among allulose and fructose difference was not distinguishable. This may be the reason behind fructose's water structure breaking properties stated in literature (Mredha et

al., 2013) . Mathlouthi & Seuvre (1988), stated that glucose had higher viscosity at the same concentration with respect to fructose. Also, when the RAMAN spectrum of pure water, fructose and glucose were compared, noticeable change in the spectrum was observed for fructose indicating the water structure breaker properties of fructose was more recognized than glucose (Birch & Shamil, 1988). Besides, studies concerning the allulose shown that, in pectin-based gel structures, allulose was found to be inefficient to dehydrate the system due to its poor water binding properties (Ates et al., 2021). In that regard, findings inferring that the superiority of glucose and poor water binding ability of allulose is compatible with the experimental outputs.

Difference in the hydration behavior brings the concept of solubility to discussion. Solubility of glucose, fructose and allulose were found to be 50%, 80% and 72% at 25^{o}C. Considering that the better hydration properties of glucose, it can be pointed out that improved water interactions may not be the basis while describing the solubility of a monomer. The concept of solubility requires deeper investigation (Maugeri et al., 2017).

3.4.1.4 Comparison Between Fructose and Allulose

Since fructose and allulose are C3 epimers of each other they have the exact configuration beside the third carbon. Results showed that in pyranose forms of fructose and allulose; peak heights were lower for allulose, the change being higher in *O1*, *O3* and *O5*, as in Figure 3.12. Also, in furanose forms minor reductions in the peak heights took place, being mostly recognized in *O3* and *O4* but not considered to be much in comparison with the changes in pyranoses. RDF results together with HB analysis revealed that, configurational changes between fructose to allulose significantly affected the water interaction ability of allulose pyranoses. It can be hypothesized that, *O1, O3* and *O5* was responsible from the decrease observed in number of sugar-water HBs as pictured in Figure 3.4C and 3.4D. Also, the reason behind the decreased water clustering of the stated oxygens was in accordance with

the more frequent occurrence of intramolecular HBs observed in allulose pyranoses in comparison with fructose pyranoses. It can be hypothesized that, C3 epimerization of fructose improved the ability of pyranose to form the intramolecular HBs while decreases the intramolecular H-Bonding in furanose forms. This may result; (1) more frequent formation of furanose form in aqueous solution, even though it is widely accepted that pyranose forms better interact with water and (2) decreased overall water interactions in allulose (Eliasson, 2017). Supportively, in a conformational study of monomers in aqueous solution, results revealed that, none of the abundant conformations of monosaccharides contained intramolecular HBs (Gaweda & Plazinski, 2019). Epimerization by resulting frequent appearance of even a single intramolecular bond may change the tautomerization mechanism and aqueous behavior of the molecule

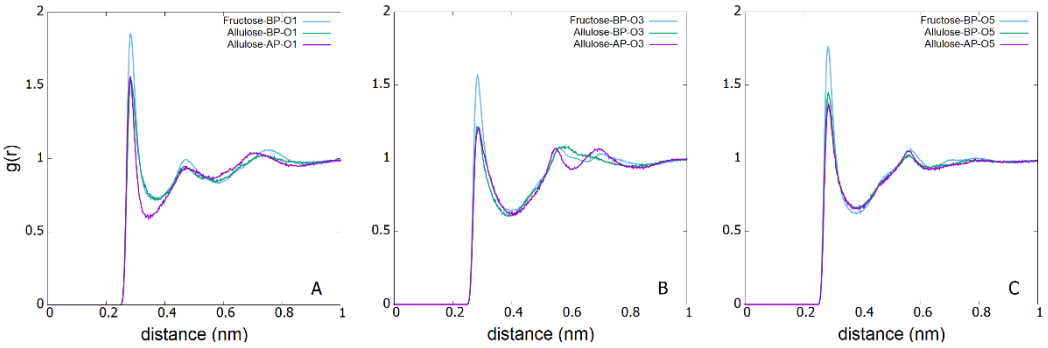

Figure 3.12. Radial Distribution Functions of water oxygens around *O1* (A), *O3* (B) and *O5* (C) of fructose and allulose at 40% (w/w) concentration. α-pyranose, BP: β-pyranose, AF: α-furanose, BF: β-furanose

CHAPTER 4

CONCLUSION

MD simulations of aqueous glucose, fructose and allulose solutions were successfully performed for 10, 20 and 40 % (w/w) systems, with good equilibration and stabilization properties and, high representability. Interaction analysis of the systems revealed that, while the number of intermolecular sugar-sugar HBs was around 1 and observed approximately in 1% of the trajectory for all systems, 7 to 9.5 sugar-water HBs per sugar molecule formed in 100% of the trajectory, the number was dominated by glucose, followed by fructose and allulose. Even the number of intramolecular bonds were around 1 for all sugar molecules in the study, the occurrence frequency was considerably higher for the allulose pyranoses followed by allulose furanoses, and fructose furanoses. RDF outputs were in good agreement with the HB analysis. It was revealed that among glucose anomers β glucose had better water clustering ability. Among fructose anomers and tautomers, no significant difference was observed and, for the allulose, furanoses were better interacting with water than pyranoses. Among all sugars, glucose was the best to cluster water molecules around and form HBs while allulose was the one with least water clustering and H-Bonding abilities. Water HB lattice disruption observed to be minor in glucose and more pronounced in fructose and allulose, especially for the furanose forms. Finally, it was revealed that, the main difference between the fructose and allulose, i.e., C3 epimers, the intramolecular HB forming tendency of allulose improved espeicially in pyranose forms. Hence it was hypothesized to be related with the decreased water interactions. Regardig diffusion coefficients, sugar and water diffusion coefficients were in a decrease being in a good agreement with the increase in the ratio of bound water molecules with increasing concentration, This was consistent with 100% presence of sugar-water HBs in all systems resulting more HBs with increasing concentration, hence hindering the mobility. With all

findings considered together, some distinct hydration behaviors of isomeric monosaccharides were revealed. Hydration behavior, related with the sugar-sugar and sugar-water interactions are critical for the food properties as water activity, solubility, glass transition temperature, melting temperature, and osmotic pressure. Hence the study contributes into the predictability of the processing or storage conditions, and material's compatibility of the new formulations. Also, water D-allulose interaction was successfully simulated by MD approach for the first time in such a detailed analysis.

REFERENCES

Abraham, M., Hess, B., van der Spoel, D., & Lindahl, E. (2016). *GROMACS Reference Manual Version 5.1.4*. https://doi.org/10.1093/cid/ciq238

Abraham, M., Murtola, T., Schulz, R., Páll, S., Smith, J. C., Hess, B., & Lindah, E. (2015). Gromacs: High performance molecular simulations through multi-level parallelism from laptops to supercomputers. *SoftwareX*, *1–2*, 19–25. https://doi.org/10.1016/j.softx.2015.06.001

American Chemical Society. (2017). *Fructose*. Molecule of the Week Archive. https://www.acs.org/content/acs/en/molecule-of-the-week/archive/f/fructose.html

Ates, E. G., Ozvural, E. B., & Oztop, M. H. (2021). Understanding the role of d-Allulose and soy protein addition in pectin gels. *Journal of Applied Polymer Science*, *138*(8). https://doi.org/10.1002/app.49885

Ben Gaïda, L., Dussap, C. G., & Gros, J. B. (2006). Variable hydration of small carbohydrates for predicting equilibrium properties in diluted and concentrated solutions. *Food Chemistry*, *96*(3), 387–401. https://doi.org/10.1016/j.foodchem.2005.02.053

Berendsen, H. J. C. (1991). Transport Properties Computed by Linear Response through Weak Coupling to a Bath. In M. Meyer & V. Pontikis (Eds.), *Computer Simulation in Materials Science* (pp. 139–155). Springer. https://doi.org/https://doi.org/10.1007/978-94-011-3546-7_7

Berman, H. M., Battistuz, T., Bhat, T. N., Bluhm, W. F., Bourne, P. E., Burkhardt, K., Feng, Z., Gilliland, G. L., Iype, L., Jain, S., Fagan, P., Marvin, J., Padilla, D., Ravichandran, V., Schneider, B., Thanki, N., Weissig, H., Westbrook, J. D., & Zardecki, C. (2002). The protein data bank. *Acta Crystallographica Section D: Biological Crystallography*, *58*(6 I), 899–907. https://doi.org/10.1107/S0907444902003451

Birch, G. G., & Shamil, S. (1988). Structure, sweetness and solution properties of small carbohydrate molecules. *Journal of the Chemical Society, Faraday Transactions 1: Physical Chemistry in Condensed Phases*, *84*(8), 2635–2640. https://doi.org/10.1039/F19888402635

Bordat, P., Lerbret, A., Demaret, J. P., Affouard, F., & Descamps, M. (2004). Comparative study of trehalose, sucrose and maltose in water solutions by molecular modelling. *Europhysics Letters*, *65*(1), 41–47. https://doi.org/10.1209/epl/i2003-10052-0

Braun, E., Gilmer, J., Mayes, H. B., Mobley, D. L., Monroe, J. I., Prasad, S., & Zuckerman, D. M. (2019). Best Practices for Foundations in Molecular Simulations [Article v1.0]. *Living Journal of Computational Molecular Science*, *1*(1), 1–28. https://doi.org/10.33011/livecoms.1.1.5957

Bullerjahn, J. T., Von Bülow, S., & Hummer, G. (2020). Optimal estimates of self-diffusion coefficients from molecular dynamics simulations. *Journal of Chemical Physics*, *153*(2). https://doi.org/10.1063/5.0008312

Chen, F., & Smith, P. E. (2007). Simulated surface tensions of common water models. *Journal of Chemical Physics*, *126*(22). https://doi.org/10.1063/1.2745718

Darden, T., York, D., & Pedersen, L. (1993). Particle mesh Ewald: An N·log(N) method for Ewald sums in large systems. *The Journal of Chemical Physics*, *98*(12), 10089–10092. https://doi.org/10.1063/1.464397

Ekdawi-Sever, N. C., Conrad, P. B., & De Pablo, J. J. (2001). Molecular simulation of sucrose solutions near the glass transition temperature. *Journal of Physical Chemistry A*, *105*(4), 734–742. https://doi.org/10.1021/jp002722i

Ekdawi-Sever, N., De Pablo, J. J., Feick, E., & Von Meerwall, E. (2003). Diffusion of sucrose and α,α-trehalose in aqueous solutions. *Journal of Physical Chemistry A*, *107*(6), 936–943. https://doi.org/10.1021/jp020187b

El Khadem, H. S. (1988). Carbohydrate chemistry: Monosaccharides and their oligomers. In *Academic Press* (Vol. 218). https://doi.org/10.1016/s0003-2670(00)80317-7

Eliasson, A. C. (2017). *Carbohydrates in Food* (3rd ed.). CRC Press/Taylor & Francis.

Engelsen, S. B., Monteiro, C., Hervé De Penhoat, C., & Pérez, S. (2001). The diluted aqueous solvation of carbohydrates as inferred from molecular dynamics simulations and NMR spectroscopy. *Biophysical Chemistry*, *93*(2–3), 103–127. https://doi.org/10.1016/S0301-4622(01)00215-0

Fennema, O. R. (1996). Food Chemistry. In *Scientific Evidence for Musculoskeletal, Bariatric, and Sports Nutrition*. Marcel Dekker. https://doi.org/10.5005/jp/books/12611_4

Franks, F. (1987). Physical chemistry of small carbohydrates— equilibrium solution properties. *Pure and Applied Chemistry*, *59*(9), 1189–1202. https://doi.org/10.1351/pac198759091189

Fukada, K., Ishii, T., Tanaka, K., Yamaji, M., Yamaoka, Y., Kobashi, K. I., & Izumori, K. (2010). Crystal structure, solubility, and mutarotation of the rare monosaccharide D-psicose. *Bulletin of the Chemical Society of Japan*, *83*(10), 1193–1197. https://doi.org/10.1246/bcsj.20100148

Galema, S. A., & Høiland, H. (1991). Stereochemical aspects of hydration of carbohydrates in aqueous solutions. 3. Density and ultrasound measurements. *Journal of Physical Chemistry*, *95*(13), 5321–5326. https://doi.org/10.1021/j100166a073

Gaweda, K., & Plazinski, W. (2017). Pyranose ring conformations in mono- and oligosaccharides: A combined MD and DFT approach. *Physical Chemistry Chemical Physics*, *19*(31), 20760–20772. https://doi.org/10.1039/c7cp02920a

Gaweda, K., & Plazinski, W. (2019). Tautomeric and epimeric equilibria of aldo-

and ketohexoses studied by the MD simulations and QM calculations. *Carbohydrate Research*, *474*(November 2018), 8–15. https://doi.org/10.1016/j.carres.2019.01.004

Gharsallaoui, A., Rogé, B., Génotelle, J., & Mathlouthi, M. (2008). Relationships between hydration number, water activity and density of aqueous sugar solutions. *Food Chemistry*, *106*(4 SPEC. ISS.), 1443–1453. https://doi.org/10.1016/j.foodchem.2007.02.047

Hanwell, M. D., Curtis, D. E., Lonie, D. C., Vandermeersch, T., Zurek, E., & Hutchison, G. (2012). Avogadro: an advanced semantic chemical editor, visualization, and analysis platform. *Journal of Cheminformatics*, *4*(17), 1–17. https://doi.org/10.1016/j.aim.2014.05.019

Hatcher, E., Guvench, O., & MacKerell, A. D. (2009). Charmm additive all-atom force field for aldopentofuranoses, methyl-aldopentofuranosides, and fructofuranose. *Journal of Physical Chemistry B*, *113*(37), 12466–12476. https://doi.org/10.1021/jp905496e

Heid, E., Honegger, P., Braun, D., Szabadi, A., Stankovic, T., Steinhauser, O., & Schröder, C. (2019). Computational spectroscopy of trehalose, sucrose, maltose, and glucose: A comprehensive study of TDSS, NQR, NOE, and DRS. *Journal of Chemical Physics*, *150*(17). https://doi.org/10.1063/1.5095058

Hoover, W. (1985). Canonical dynamics: Equilibrium phase-space distributions. *Physical Review*, *31*(3), 1695–1697.

Huang, J., Rauscher, S., Nawrocki, G., Ran, T., Feig, M., De Groot, B. L., Grubmüller, H., & MacKerell, A. D. (2016). CHARMM36m: An improved force field for folded and intrinsically disordered proteins. *Nature Methods*, *14*(1), 71–73. https://doi.org/10.1038/nmeth.4067

International Society of Rare Sugars. (2019). *Definition of Rare Sugars*. http://www.isrs.kagawa-u.ac.jp/definition.html

Izydorczyk, M. (2005). Understanding the Chemistry of Food Carbohydrates. In S. W. Cui (Ed.), *Food Carbohydrates*. CRC Press. https://doi.org/10.1201/9780203485286.ch1

Jo, S., Kim, T., Iyer, V. G., & Im, W. (2008). Software News and Updates CHARMM-GUI: A Web-Based Graphical User Interface for CHARMM. *Journal of Computational Chemistry*, *29*(11), 1859–1865. https://doi.org/10.1002/jcc

Knapp, B., Frantal, S., Cibena, M., Schreiner, W., & Bauer, P. (2011). Is an intuitive convergence definition of molecular dynamics simulations solely based on the root mean square deviation possible? *Journal of Computational Biology*, *18*(8), 997–1005. https://doi.org/10.1089/cmb.2010.0237

Köpper, S., & Freimund, S. (2003). The composition of keto aldoses in aqueous solution as determined by NMR spectroscopy. *Helvetica Chimica Acta*, *86*(3), 827–843. https://doi.org/10.1002/hlca.200390083

Kozakai, T., Fukada, K., Kuwatori, R., Ishii, T., Senoo, T., & Izumori, K. (2015). Aqueous phase behavior of the rare monosaccharide D-allose and X-ray crystallographic analysis of D-allose dihydrate. *Bulletin of the Chemical Society of Japan*, *88*(3), 465–470. https://doi.org/10.1246/bcsj.20140337

Kräutler, V., Van Gunsteren, W. F., & Hünenberger, P. H. (2001). A fast SHAKE algorithm to solve distance constraint equations for small molecules in molecular dynamics simulations. *Journal of Computational Chemistry*, *22*(5), 501–508. https://doi.org/10.1002/1096-987X(20010415)22:5<501::AID-JCC1021>3.0.CO;2-V

Laage, D., & Hynes, J. T. (2008). On the molecular mechanism of water reorientation. *Journal of Physical Chemistry B*, *112*(45), 14230–14242. https://doi.org/10.1021/jp805217u

Leach, A. R. (2001). *Molecular modelling _ principles and applications-Prentice Hall (2001).pdf* (pp. 1–744).

Lee, S. L., Debenedetti, P. G., & Errington, J. R. (2005). A computational study of hydration, solution structure, and dynamics in dilute carbohydrate solutions. *Journal of Chemical Physics*, *122*(20). https://doi.org/10.1063/1.1917745

Lerbret, A., Bordat, P., Affouard, F., Descamps, M., & Migliardo, F. (2005). How homogeneous are the trehalose, maltose, and sucrose water solutions? An insight from molecular dynamics simulations. *Journal of Physical Chemistry B*, *109*(21), 11046–11057. https://doi.org/10.1021/jp0468657

Lesar, R. (2013). *Introduction to Computaional Material Sciences* (R. Lesar (ed.); 1st ed.). Cambridge University Press.

Li, C., Lin, J., Guo, Q., Zhang, C., Du, K., Lin, H., & Lin, J. (2018). D-psicose 3-epimerase secretory overexpression, immobilization, and d-psicose biotransformation, separation and crystallization. *Journal of Chemical Technology and Biotechnology*, *93*(2), 350–357. https://doi.org/10.1002/jctb.5360

Livingstone, G., Franks, F., & Aspinall, L. J. (1977). The effects of aqueous solvent structure on the mutarotation kinetics of glucose. *Journal of Solution Chemistry*, *6*(3), 203–216. https://doi.org/10.1007/BF00646739

Ma, Y., Zhang, B., Li, H., Li, Y., Hu, J., Li, J., Wang, H., & Deng, Z. (2017). Chemical and molecular dynamics analysis of crystallization properties of honey. *International Journal of Food Properties*, *20*(4), 725–733. https://doi.org/10.1080/10942912.2016.1178282

MacKerell, A. D., Raman, E. P., & Guvench, O. (2010). CHARMM additive all-atom force field for glycosidic linkages in carbohydrates involving furanoses. *Journal of Physical Chemistry B*, *114*(40), 12981–12994. https://doi.org/10.1021/jp105758h

Maginn, E. J., Messerly, R. A., Carlson, D. J., Roe, D. R., & Elliott, J. R. (2019). Best Practices for Computing Transport Properties 1. Self-Diffusivity and Viscosity from Equilibrium Molecular Dynamics [Article v1.0]. *Living*

Journal of Computational Molecular Science, *1*(1), 1–20. https://doi.org/10.33011/livecoms.1.1.6324

Mark, P., & Nilsson, L. (2001). Structure and dynamics of the TIP3P, SPC, and SPC/E water models at 298 K. *Journal of Physical Chemistry A*, *105*(43), 9954–9960. https://doi.org/10.1021/jp003020w

Mathlouthi, M., & Seuvre, A. M. (1988). Solution properties and the sweet taste of small carbohydrates. *Journal of the Chemical Society, Faraday Transactions 1: Physical Chemistry in Condensed Phases*, *84*(8), 2641–2650. https://doi.org/10.1039/F19888402641

Matlouthi, M., & Reiser, P. (1995). *Sucrose Properties and Applications*. Springer.

Maugeri, L., Busch, S., McLain, S. E., Pardo, L. C., Bruni, F., & Ricci, M. A. (2017). Structure-activity relationships in carbohydrates revealed by their hydration. *Biochimica et Biophysica Acta - General Subjects*, *1861*(6), 1486–1493. https://doi.org/10.1016/j.bbagen.2016.12.017

Molteni, C., & Parrinello, M. (1998). Glucose in aqueous solution by first principles molecular dynamics. *Journal of the American Chemical Society*, *120*(9), 2168–2171. https://doi.org/10.1021/ja973008q

Mredha, M. T. I., Roy, C. K., Rahman, M. M., Mollah, M. Y. A., & Susan, M. A. B. H. (2013). An electrochemical approach to study water-d(-)fructose interactions. *Electrochimica Acta*, *97*, 231–237. https://doi.org/10.1016/j.electacta.2013.02.123

Naik, R. R., Gandhi, N. S., Thakur, M., & Nanda, V. (2019). Analysis of crystallization phenomenon in Indian honey using molecular dynamics simulations and artificial neural network. *Food Chemistry*, *300*(May), 125182. https://doi.org/10.1016/j.foodchem.2019.125182

Neuman, R. C. (2013). Organic Chemistry. In *Organic Chemistry*. http://web.chem.ucsb.edu/~neuman/orgchembyneuman/BookContents.html

Nosé, S. (1984). A molecular dynamics method for simulations in the canonical ensemble. *Molecular Physics*, *52*(2), 255–268. https://doi.org/10.1080/00268978400101201

Pamies, S. C., Petelski, A. N., Castro, E. A., & Sosa, G. L. (2017). Static and Dynamic Study of Disaccharides Trehalose, Maltose and Sucrose. *Structural Chemistry*, *28*(4), 911–924. https://doi.org/10.1007/s11224-016-0896-5

Pandey, P., & Mallajosyula, S. S. (2016). Influence of polarization on carbohydrate hydration: A comparative study using additive and polarizable force fields. *Journal of Physical Chemistry B*, *120*(27), 6621–6633. https://doi.org/10.1021/acs.jpcb.6b05546

Paolantoni, M., Comez, L., Fioretto, D., Gallina, M. E., Morresi, A., Sassi, P., & Scarponi, F. (2008). Structural and dynamical properties of glucose aqueous solutions by depolarized Rayleigh scattering. *Journal of Raman Spectroscopy*, *39*, 238–249. https://doi.org/10.1002/jrs.1909

Park, S. J., Lee, J., Qi, Y., Kern, N. R., Lee, H. S., Jo, S., Joung, I., Joo, K., Lee, J., & Im, W. (2019). CHARMM-GUI Glycan Modeler for modeling and simulation of carbohydrates and glycoconjugates. *Glycobiology*, *29*(4), 320–331. https://doi.org/10.1093/glycob/cwz003

Parrinello, M., & Rahman, A. (1981). Polymorphic transitions in single crystals: A new molecular dynamics method. *Journal of Applied Physics*, *52*(12).

Petrova, S. S., & Solov'Ev, A. D. (1997). The Origin of the Method of Steepest Descent. *Historia Mathematica*, *24*(4), 361–375. https://doi.org/10.1006/hmat.1996.2146

Plazinski, W., & Plazinska, A. (2017). Molecular dynamics simulations of hexopyranose ring distortion in different force fields. *Pure and Applied Chemistry*, *89*(9), 1283–1294. https://doi.org/10.1515/pac-2016-0922

Plazinski, W., Plazinska, A., & Drach, M. (2016). Acyclic forms of aldohexoses

and ketohexoses in aqueous and DMSO solutions: Conformational features studied using molecular dynamics simulations. *Physical Chemistry Chemical Physics*, *18*(14), 9626–9635. https://doi.org/10.1039/c6cp00809g

Pocan, P., Ilhan, E., Florek–Wojciechowska, M., Masiewicz, E., Kruk, D., & Oztop, M. H. (2021). Exploring the water mobility in gelatin based soft candies by means of Fast Field Cycling (FFC) Nuclear Magnetic Resonance relaxometry. *Journal of Food Engineering*, *294*(December 2020). https://doi.org/10.1016/j.jfoodeng.2020.110422

Pomata, M. H. H., Sonoda, M. T., Skaf, M. S., & Dolores Elola, M. (2009). Anomalous dynamics of hydration water in carbohydrate solutions. *Journal of Physical Chemistry B*, *113*(39), 12999–13006. https://doi.org/10.1021/jp904019c

Rampp, M., Buttersack, C., & Lüdemann, H. D. (2000). c,T-dependence of the viscosity and the self-diffusion coefficients in some aqueous carbohydrate solutions. *Carbohydrate Research*, *328*(4), 561–572. https://doi.org/10.1016/S0008-6215(00)00141-5

Rapaport, D. C. (1995). The Art of Molecular Dynamic Simulations. In *Journal of Petrology* (Vol. 369, Issue 1). Cambridge University Press. https://doi.org/10.1017/CBO9781107415324.004

Schenk, F. W. (1998). Glucose and Glucose-Containing Syrups. *Ullmann's Encyclopedia of Industrial Chemistry*, *16*, 67–82. https://doi.org/10.1002/14356007.a12

Shiraga, K., Suzuki, T., Kondo, N., De Baerdemaeker, J., & Ogawa, Y. (2015). Quantitative characterization of hydration state and destructuring effect of monosaccharides and disaccharides on water hydrogen bond network. *Carbohydrate Research*, *406*, 46–54. https://doi.org/10.1016/j.carres.2015.01.002

Silva, A. M., da Silva, E. C., & da Silva, C. O. (2006). A theoretical study of

glucose mutarotation in aqueous solution. *Carbohydrate Research*, *341*(8), 1029–1040. https://doi.org/10.1016/j.carres.2006.02.035

Sonoda, M. T., & Skaf, M. S. (2007). Carbohydrate clustering in aqueous solutions and the dynamics of confined water. *Journal of Physical Chemistry B*, *111*(41), 11948–11956. https://doi.org/10.1021/jp0749120

Talon, C., Smith, L. J., Brady, J. W., Lewis, B. A., Copley, J. R. D., Price, D. L., & Saboungi, M. L. (2004). Dynamics of Water Molecules in Glucose Solutions. *Journal of Physical Chemistry B*, *108*(16), 5120–5126. https://doi.org/10.1021/jp035161e

Van Gunsteren, W. F., & Berendsen, H. J. C. (1988). A Leap-frog Algorithm for Stochastic Dynamics. *Journal of Molecular Simulation*, *1*(3), 173–185.

Von Bülow, S., Bullerjahn, J. T., & Hummer, G. (2020). Systematic errors in diffusion coefficients from long-time molecular dynamics simulations at constant pressure. *Journal of Chemical Physics*, *153*(2). https://doi.org/10.1063/5.0008316

Wrolstad, R. E. (2012). *Food Carbohydrate Chemistry*. Wiley-Blackwell.

APPENDICES

A. Time Evolution of Simulation Energetics

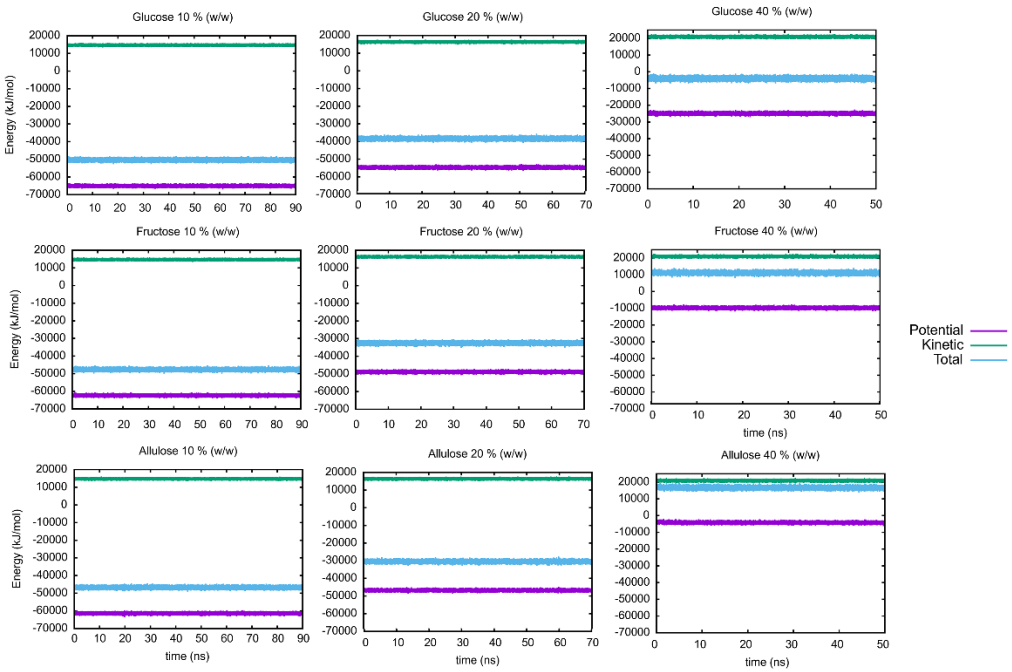

Figure 4.1. Time evolution of energies in each system

B. Time Evolution of RMSD

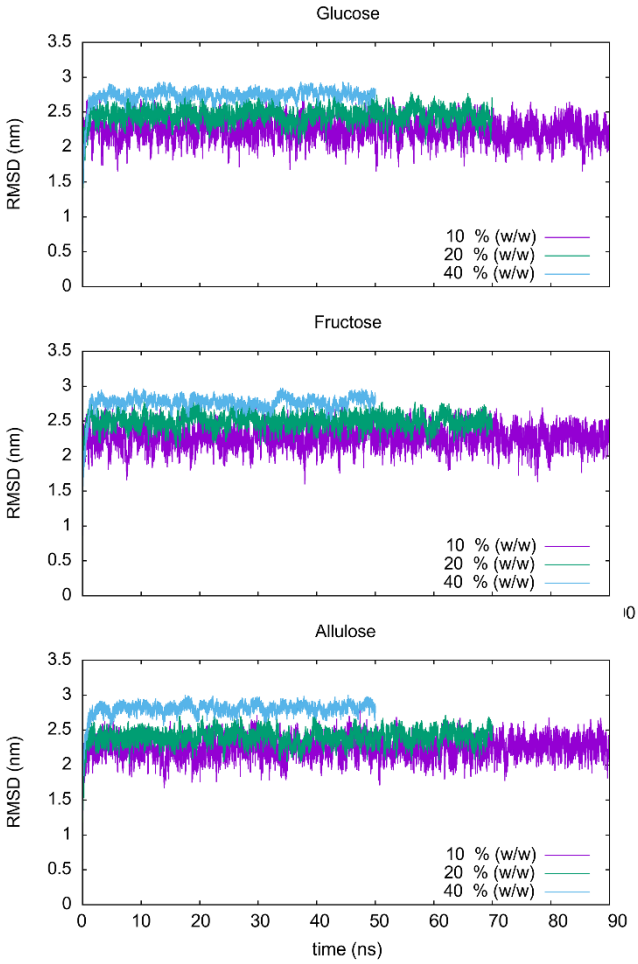

Figure 4.2. Time evolution of Root Mean Squared Deviation in Glucose, Fructose and Allulose systems

C. Structure Files of Self Drawn Molecules

Structure file of α-D-psicopyranose

```
COMPND    UNNAMED
AUTHOR    GENERATED BY OPEN BABEL 2.3.90
HETATM    1  O   UNL A   1      -0.905  -0.559  -0.720  1.00  0.00
O
HETATM    2  C   UNL A   1      -1.875  -1.105   0.173  1.00  0.00
C
HETATM    3  C   UNL A   1       0.428  -1.046  -0.542  1.00  0.00
C
HETATM    4  C   UNL A   1      -1.990  -2.632   0.057  1.00  0.00
C
HETATM    5  H   UNL A   1      -2.835  -0.631  -0.059  1.00  0.00
H
HETATM    6  H   UNL A   1      -1.601  -0.813   1.193  1.00  0.00
H
HETATM    7  C   UNL A   1       0.506  -2.378   0.256  1.00  0.00
C
HETATM    8  C   UNL A   1      -0.631  -3.297  -0.214  1.00  0.00
C
HETATM    9  O   UNL A   1       0.931  -1.331  -1.864  1.00  0.00
O
HETATM   10  H   UNL A   1       1.766  -0.820  -1.922  1.00  0.00
H
HETATM   11  O   UNL A   1       1.762  -3.040   0.087  1.00  0.00
O
HETATM   12  H   UNL A   1       0.383  -2.188   1.329  1.00  0.00
H
HETATM   13  H   UNL A   1       1.859  -3.178  -0.877  1.00  0.00
H
HETATM   14  O   UNL A   1      -0.517  -3.612  -1.621  1.00  0.00
O
```

```
HETATM   15  H   UNL A   1      -0.579  -4.263   0.301  1.00  0.00
H
HETATM   16  H   UNL A   1      -0.205  -2.802  -2.083  1.00  0.00
H
HETATM   17  O   UNL A   1      -2.928  -2.988  -0.965  1.00  0.00
O
HETATM   18  H   UNL A   1      -2.404  -3.003   1.001  1.00  0.00
H
HETATM   19  H   UNL A   1      -2.399  -3.406  -1.678  1.00  0.00
H
HETATM   20  C   UNL A   1       1.283   0.083   0.080  1.00  0.00
C
HETATM   21  O   UNL A   1       2.664  -0.098  -0.232  1.00  0.00
O
HETATM   22  H   UNL A   1       1.148   0.128   1.166  1.00  0.00
H
HETATM   23  H   UNL A   1       0.983   1.053  -0.333  1.00  0.00
H
HETATM   24  H   UNL A   1       3.164   0.556   0.288  1.00  0.00
H
CONECT    1    2    3
CONECT    2    1    4    5    6
CONECT    3    1    7    9   20
CONECT    4    2    8   17   18
CONECT    5    2
CONECT    6    2
CONECT    7    3    8   11   12
CONECT    8    4    7   14   15
CONECT    9    3   10
CONECT   10    9
CONECT   11    7   13
```

```
CONECT   12    7
CONECT   13   11
CONECT   14    8   16
CONECT   15    8
CONECT   16   14
CONECT   17    4   19
CONECT   18    4
CONECT   19   17
CONECT   20    3   21   22   23
CONECT   21   20   24
CONECT   22   20
CONECT   23   20
CONECT   24   21
MASTER        0    0    0    0    0    0    0    0   24    0   24
0
END
```

Structure file of β-D-psicopyranose

```
COMPND    UNNAMED
AUTHOR    GENERATED BY OPEN BABEL 2.3.90
HETATM    1  O   UNL A   1      -0.584  -0.500  -1.124  1.00  0.00
O
HETATM    2  C   UNL A   1      -1.560  -0.943  -0.185  1.00  0.00
C
HETATM    3  C   UNL A   1       0.757  -0.888  -0.793  1.00  0.00
C
HETATM    4  C   UNL A   1      -1.710  -2.469  -0.223  1.00  0.00
C
HETATM    5  H   UNL A   1      -2.508  -0.457  -0.439  1.00  0.00
H
```

```
HETATM    6  H   UNL A   1      -1.268  -0.603   0.816  1.00  0.00
H
HETATM    7  C   UNL A   1       0.811  -2.319  -0.166  1.00  0.00
C
HETATM    8  C   UNL A   1      -0.390  -3.177  -0.575  1.00  0.00
C
HETATM    9  O   UNL A   1       1.298   0.047   0.147  1.00  0.00
O
HETATM   10  H   UNL A   1       2.103  -0.363   0.513  1.00  0.00
H
HETATM   11  O   UNL A   1       2.046  -2.988  -0.449  1.00  0.00
O
HETATM   12  H   UNL A   1       0.784  -2.214   0.927  1.00  0.00
H
HETATM   13  H   UNL A   1       1.922  -3.427  -1.317  1.00  0.00
H
HETATM   14  O   UNL A   1      -0.361  -3.528  -1.971  1.00  0.00
O
HETATM   15  H   UNL A   1      -0.349  -4.139  -0.051  1.00  0.00
H
HETATM   16  H   UNL A   1      -0.038  -2.753  -2.486  1.00  0.00
H
HETATM   17  O   UNL A   1      -2.728  -2.853  -1.156  1.00  0.00
O
HETATM   18  H   UNL A   1      -2.057  -2.791   0.765  1.00  0.00
H
HETATM   19  H   UNL A   1      -2.256  -3.259  -1.914  1.00  0.00
H
HETATM   20  C   UNL A   1       1.584  -0.751  -2.094  1.00  0.00
C
HETATM   21  O   UNL A   1       1.214  -1.729  -3.072  1.00  0.00
O
HETATM   22  H   UNL A   1       2.657  -0.848  -1.894  1.00  0.00
H
```

```
HETATM   23  H   UNL A   1       1.420   0.241  -2.534  1.00  0.00
H
HETATM   24  H   UNL A   1       1.639  -1.451  -3.906  1.00  0.00
H
CONECT    1    2    3
CONECT    2    1    4    5    6
CONECT    3    1    7    9   20
CONECT    4    2    8   17   18
CONECT    5    2
CONECT    6    2
CONECT    7    3    8   11   12
CONECT    8    4    7   14   15
CONECT    9    3   10
CONECT   10    9
CONECT   11    7   13
CONECT   12    7
CONECT   13   11
CONECT   14    8   16
CONECT   15    8
CONECT   16   14
CONECT   17    4   19
CONECT   18    4
CONECT   19   17
CONECT   20    3   21   22   23
CONECT   21   20   24
CONECT   22   20
CONECT   23   20
CONECT   24   21
```

```
MASTER        0    0    0    0    0    0    0    0   24    0   24
0

END
```

Structure file of β-D-psicofuranose

```
COMPND    UNNAMED

AUTHOR    GENERATED BY OPEN BABEL 2.3.90

HETATM    1  C   UNL A   1      -0.370   0.117   0.366  1.00  0.00
C

HETATM    2  C   UNL A   1       0.757  -0.910   0.454  1.00  0.00
C

HETATM    3  C   UNL A   1      -0.008  -2.155   0.885  1.00  0.00
C

HETATM    4  C   UNL A   1      -1.314  -1.997   0.071  1.00  0.00
C

HETATM    5  O   UNL A   1      -1.546  -0.585  -0.078  1.00  0.00
O

HETATM    6  C   UNL A   1      -0.071   1.278  -0.585  1.00  0.00
C

HETATM    7  H   UNL A   1      -0.575   0.528   1.363  1.00  0.00
H

HETATM    8  O   UNL A   1      -0.134  -2.078   2.318  1.00  0.00
O

HETATM    9  H   UNL A   1       0.536  -3.075   0.649  1.00  0.00
H

HETATM   10  H   UNL A   1      -1.095  -2.094   2.531  1.00  0.00
H

HETATM   11  O   UNL A   1       1.752  -0.543   1.405  1.00  0.00
O

HETATM   12  H   UNL A   1       1.470  -0.966   2.245  1.00  0.00
H

HETATM   13  O   UNL A   1       1.104   2.001  -0.250  1.00  0.00
O
```

```
HETATM   14  H   UNL A   1      -0.915   1.976  -0.593  1.00  0.00
H
HETATM   15  H   UNL A   1       0.035   0.913  -1.612  1.00  0.00
H
HETATM   16  C   UNL A   1      -2.557  -2.643   0.715  1.00  0.00
C
HETATM   17  O   UNL A   1      -2.723  -2.253   2.084  1.00  0.00
O
HETATM   18  H   UNL A   1      -2.486  -3.736   0.679  1.00  0.00
H
HETATM   19  H   UNL A   1      -3.457  -2.343   0.167  1.00  0.00
H
HETATM   20  H   UNL A   1      -3.637  -2.494   2.327  1.00  0.00
H
HETATM   21  H   UNL A   1       1.231  -1.063  -0.522  1.00  0.00
H
HETATM   22  O   UNL A   1      -1.179  -2.545  -1.239  1.00  0.00
O
HETATM   23  H   UNL A   1       1.242   1.944   0.714  1.00  0.00
H
HETATM   24  H   UNL A   1      -0.469  -2.059  -1.686  1.00  0.00
H
CONECT    1    2    5    6    7
CONECT    2    1    3   11   21
CONECT    3    2    4    8    9
CONECT    4    3    5   16   22
CONECT    5    1    4
CONECT    6    1   13   14   15
CONECT    7    1
CONECT    8    3   10
CONECT    9    3
```

```
CONECT   10    8
CONECT   11    2   12
CONECT   12   11
CONECT   13    6   23
CONECT   14    6
CONECT   15    6
CONECT   16    4   17   18   19
CONECT   17   16   20
CONECT   18   16
CONECT   19   16
CONECT   20   17
CONECT   21    2
CONECT   22    4   24
CONECT   23   13
CONECT   24   22
MASTER        0    0    0    0    0    0    0    0   24    0   24
0
END
```

D. Supporting RDF Figures

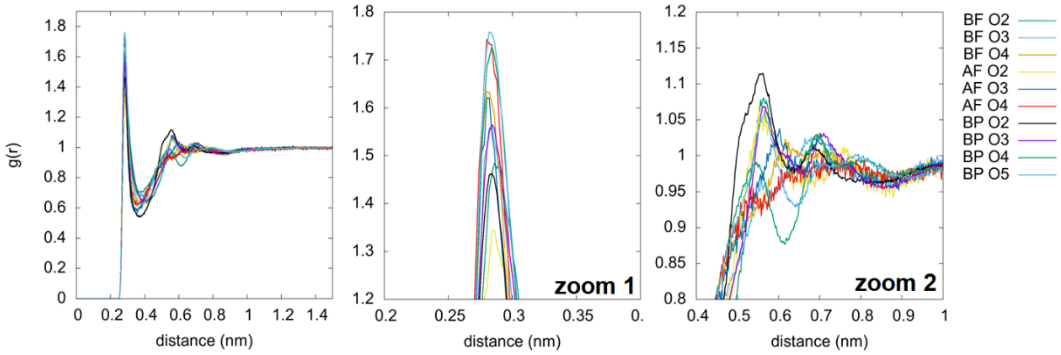

Figure 4.3. Radial Distribution of ring hydroxyl oxygens of fructose at 40% concentration (w/w)